The Astrophysical Journal, 844:171 (15pp), 2017 August 1 https://doi.org/10.3847/1538-4357/aa7d4d

Lyα Profile, Dust, and Prediction of Lyα Escape Fraction in Green Pea Galaxies

Huan Yang[1,2], Sangeeta Malhotra[2,3], Max Gronke[4], James E. Rhoads[2,3], Claus Leitherer[5], Aida Wofford[6], Tianxing Jiang[2], Mark Dijkstra[4], V. Tilvi[2], and Junxian Wang[1]
[1] CAS Key Laboratory for Research in Galaxies and Cosmology, Department of Astronomy, University of Science and Technology of China, China; huan.y@asu.edu
[2] Arizona State University, School of Earth and Space Exploration, USA
[3] NASA Goddard Space Flight Center, USA
[4] Institute of Theoretical Astrophysics, University of Oslo, Norway
[5] Space Telescope Science Institute, USA
[6] National Autonomous University of Mexico, Institute of Astronomy, Mexico
Received 2017 January 7; revised 2017 June 15; accepted 2017 June 30; published 2017 August 3

Abstract

We studied Lyman-α (Lyα) escape in a statistical sample of 43 Green Peas with *HST*/COS Lyα spectra. Green Peas are nearby star-forming galaxies with strong [O III]λ5007 emission lines. Our sample is four times larger than the previous sample and covers a much more complete range of Green Pea properties. We found that about two-thirds of Green Peas are strong Lyα line emitters with rest-frame Lyα equivalent width >20 Å. The Lyα profiles of Green Peas are diverse. The Lyα escape fraction, defined as the ratio of observed Lyα flux to intrinsic Lyα flux, shows anti-correlations with a few Lyα kinematic features—both the blue peak and red peak velocities, the peak separations, and the FWHM of the red portion of the Lyα profile. Using properties measured from Sloan Digital Sky Survey optical spectra, we found many correlations—the Lyα escape fraction generally increases at lower dust reddening, lower metallicity, lower stellar mass, and higher [O III]/[O II] ratio. We fit their Lyα profiles with the H I shell radiative transfer model and found that the Lyα escape fraction is anti-correlated with the best-fit $N_{\rm H\,I}$. Finally, we fit an empirical linear relation to predict $f_{\rm esc}^{\rm Ly\alpha}$ from the dust extinction and Lyα red peak velocity. The standard deviation of this relation is about 0.3 dex. This relation can be used to isolate the effect of intergalactic medium (IGM) scatterings from Lyα escape and to probe the IGM optical depth along the line of sight of each $z > 7$ Lyα emission-line galaxy in the *James Webb Space Telescope* era.

Key words: dark ages, reionization, first stars – galaxies: dwarf – galaxies: starburst – radiative transfer – ultraviolet: galaxies

Supporting material: machine-readable tables

1. Introduction

In young star-forming galaxies, Lyman-continuum (LyC) photons from hotstars ionize the surrounding hydrogen gas, and Lyman-α(Lyα) photons come from the recombination of hydrogen gas. The Lyα emission line is a powerful tool in discovering and studying high-redshift galaxies. Thousands of high-redshift Lyα emission-line galaxies (LAEs) have been found in the last two decades (e.g., Dey et al. 1998; Hu et al. 1998; Rhoads et al. 2000; Ouchi et al. 2003; Gawiser et al. 2006; Wang et al. 2009; Kashikawa et al. 2011; Erb et al. 2014; Matthee et al. 2014; Zheng et al. 2016). These high-redshift LAEs generally have small size, low stellar mass, low dust extinction, low metallicity, young age, and high specific star-formation rate (sSFR; e.g., Gawiser et al. 2007; Pirzkal et al. 2007; Finkelstein et al. 2008; Bond et al. 2010; Malhotra et al. 2012). At $2 \lesssim z \lesssim 6$, these LAEs are an important population of star-forming galaxies, and they constitute an increasing fraction of Lyman-break galaxies (LBGs) across that range, reaching ∼60% of LBGs at redshift $z \sim 6$ (Stark et al. 2011).

A current frontier is searching for LAEs in the epoch of cosmic reionization. As Lyα photons propagate from an LAE to the observer, they pass through the intergalactic medium (IGM) and will be scattered away from the line of sight by H I in the IGM. So, the Lyα line can be used to probe the reionization of the IGM (e.g., Malhotra & Rhoads 2004; Treu et al. 2012; Pentericci et al. 2014; Tilvi et al. 2014; Matthee et al. 2015; Santos et al. 2016). These Lyα-based methods can effectively probe the H I fraction in the latter half of reionization. One major goal of the *James Webb Space Telescope* (*JWST*) is to observe the Lyα and rest-frame optical lines spectra of $z > 7$ galaxies and to probe the reionization with the Lyα lines. However, the challenge is to isolate the impact of the IGM from the other effects that may diminish Lyα. The Lyα photons have to escape out of the galaxies before passing through the IGM and being observed, i.e., (Observed Lyα) = (Intrinsic Lyα) × (Lyα escape fraction) × (IGM Transmission). The Lyα escape fraction describes how many Lyα photons escape out of both interstellar medium (ISM) and circumgalactic medium (CGM) of an LAE. Thus, to use Lyα reionization tests, we have to understand Lyα escape and predict the Lyα escape fraction from other properties.

Lyα escape is also related to the LyC escape process. A large fraction (9/12) of known LyC leakers are LAEs (Leitet et al. 2013; Borthakur et al. 2014; de Barros et al. 2016; Izotov et al. 2016; Leitherer et al. 2016; Shapley et al. 2016). LAEs at the reionization epoch may be major contributors of ionizing photons. Lyα line profiles may be used as a tool for detecting LyC leakers (Alexandroff et al. 2015; Verhamme et al. 2015; Dijkstra et al. 2016). Understanding Lyα escape is very useful for the study of LyC escape.

As Lyα is a resonance line, it has a high cross-section for H I scattering. The emergent Lyα emission has a complicated dependence on the amount of dust, the H I gas column density ($N_{\rm H\,I}$), the kinematics of H I gas, and the geometric distribution of H I gas and dust (e.g., Neufeld 1990; Charlot & Fall 1993;

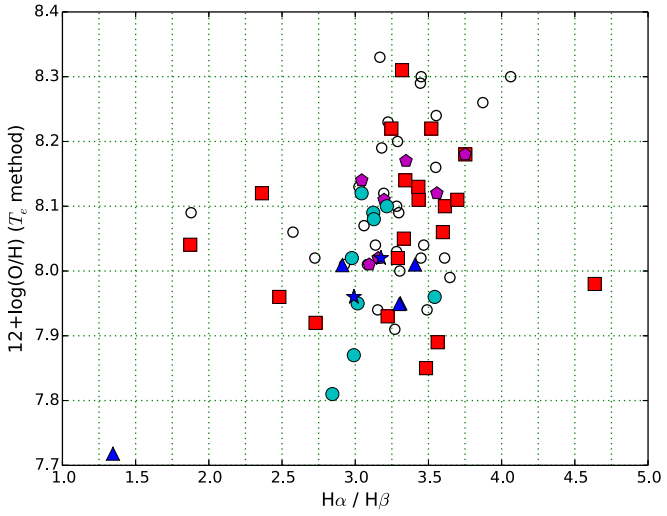

Figure 1. Metallicity and dust extinction (Hα/Hβ ratio) diagram of our Green Pea sample. Red squares show the 20 galaxies with new *HST* observations (GO 14201, PI S. Malhotra). The other samples include nine Green Pea galaxies with low dust extinction (cyan circle, Paper I; Henry et al. 2015), seven Lyman-break analog galaxies (magenta pentagon, Heckman et al. 2011; Alexandroff et al. 2015), and two Lyman-continuum leaker candidates (blue star, Jaskot & Oey et al. 2014), and give confirmed Lyman-continuum leakers (blue triangle, two blue triangles overlap; Izotov et al. 2016). The black hollow circles show the other galaxies without *HST* UV spectra in the sample of 66 Green Peas. Note that a few sources have very small Ha/Hb values. The reasons are not yet well understood, but could be due to (1) poor flat-field calibration or sky subtraction, or (2) different gas conditions from the case-B assumption.

Ahn et al. 2001; Dijkstra et al. 2006; Verhamme et al. 2006; Laursen et al. 2013). The scattering of Lyα photons can significantly modify the Lyα line profile. LAEs usually show asymmetric or double-peaked Lyα emission-line profiles (e.g., Rhoads et al. 2003; Kashikawa et al. 2011; Erb et al. 2014). Therefore, the Lyα line profile carries a lot of information about the resonant scatterings and can be used to probe the H I gas properties.

To study Lyα escape, it is ideal to have a large sample of LAEs and to measure high-quality Lyα line spectrum, many optical emission lines, H I gas properties, and multiple other galactic properties so that we can test what properties lead to Lyα escape, and finally *predict* the Lyα escape fraction from those properties. At high redshift, however, absorption by the intergalactic Lyα forest prevents reliable measurements of the blue portion of Lyα emission lines. Other crucial observations are also impractical, both because high-z LAEs are faint, and because some features (notably rest-optical emission lines) are redshifted to $\lambda_{\rm obs} > 2.4$ μm, where presently available instruments lack sensitivity. Therefore, many studies seek to solve the Lyα escape problem by observing low-z galaxies with similar properties to high-z LAEs (e.g., Giavalisco et al. 1996; Kunth et al. 1998; Mas-Hesse et al. 2003; Hayes et al. 2005, 2014; Deharveng et al. 2008; Atek et al. 2009; Finkelstein et al. 2009; Cowie et al. 2011; Heckman et al. 2011; Leitherer et al. 2011; Wofford et al. 2013; Östlin et al. 2014; Rivera-Thorsen et al. 2015). However, low-z LAEs are rare and many nearby Lyα emission-line galaxies are older and more evolved galaxies than typical high-z LAEs and may be a different population of Lyα emitters. Perhaps the most relevant nearby analogs of high-z LAEs are Green Pea galaxies (Jaskot & Oey 2014; Henry et al. 2015; Yang et al. 2016, hereafter Paper I).

Green Pea galaxies were discovered in the citizen science project Galaxy Zoo, in which public volunteers morphologically classified millions of galaxies from the Sloan Digital Sky Survey (SDSS). Green Peas are compact galaxies that are unresolved in SDSS images. The green color is because the [O III] doublet dominates the flux of the SDSS *r*-band, which is mapped to the green channel in the SDSS's false-color *gri*-band images (Lupton et al. 2004). They generally have small stellar masses ($\sim 10^{8-10} M_\odot$), low metallicities for their stellar masses, high sSFR, and large [O III]λ5007/[O II]λ3727 (hereafter [O III]/[O II]) ratio (Cardamone et al. 2009; Amorín et al. 2010; Izotov et al. 2011). The UV spectra of 17 Green Peas generally show strong Lyα emission lines (Paper I; Jaskot & Oey 2014; Henry et al. 2015; Izotov et al. 2016; Verhamme et al. 2017). These studies have explored the relation of $f_{\rm esc}^{\rm Ly\alpha}$ and dust, metallicity, Lyα profiles, and metal absorption lines with small samples of Green Peas. Besides the small sample size, previous samples of Green Peas tended to have lower metallicity and lower dust extinction than the whole Green Pea sample. In our *HST* program, we observed an additional 20 Green Peas in order to have a statistical sample that spans a range of galaxy properties such as metallicity, dust extinction, and star formation rate (SFR).

In this paper, we use *HST*/COS Lyα spectra of Green Peas to study the mechanism of Lyα escape. In Section 2, we show the sample and observations. In Section 3, we describe the measurement and properties of the Lyα equivalent width and escape fraction. In Section 4, we show the relation between Lyα escape and Lyα kinematic features. In Section 5, we show the relation between Lyα escape and dust extinction, metallicity, stellar mass, morphology, and [O III]/[O II] ratio. In Section 6, we fit the Lyα profiles with the radiative transfer model. In Section 7, we show an empirical relation to predict the Lyα escape fraction and discuss its applications for probing reionization.

2. Sample and Observations

2.1. The Sample

Since the strong [O III]λ5007 line makes Green Pea galaxies have special optical broadband colors, we can select a few thousand Green Pea candidates from the SDSS imaging survey (H. Yang et al. 2016, in preparation). In SDSS DR7, a sample of 251 Green Peas was observed as serendipitous spectroscopic targets (Cardamone et al. 2009). A subset of 66 Green Peas have sufficient signal-to-noise ratio (S/N) in both continuum and emission lines (Hα, Hβ, and [O III]λ5007) to study galactic properties such as SFR, stellar mass, and metallicity (Cardamone et al. 2009; Izotov et al. 2011). Galaxies with an active galactic nucleus (diagnosed through their broad Balmer emission lines or Hα/[N II] versus [O III]/Hβ diagram) are excluded. In Paper I, we matched these 66 Green Peas with the COS archive and studied Lyα escape in a sample of 12 Green Peas with COS UV spectra. Compared to the larger Green Pea sample, these 12 Green Peas tended to have lower metallicity and lower dust extinction (Figure 1). To address the bias and expand the sample size, we took the Lyα spectra of 20 additional Green Peas (PI S. Malhotra, GO 14201). These 20 galaxies were selected based on their metallicity and Hα/Hβ values to supplement the previous sample, so that the total sample can cover the whole range of metallicity and dust extinction of the parent sample. We use Figure 1 to do the selection by first drawing grids (shown in

Figure 1), then picking one or two sources in each grid cell. Note that (a) empty cells are not used and (b) the non-empty cells are not covered perfectly because in the proposal we used the gas metallicities measured in Izotov et al. (2011), which are slightly different from the metallicities shown in Figure 1. After the selection, we compared the total sample with the parent sample to make sure there are no obvious biases.

We also supplement this sample with 11 additional Green Peas from published literature. In total, we have 43 Green Peas from six *HST* programs—20 galaxies from GO 14201 (PI S. Malhotra), 9 galaxies from GO 12928 (PI A. Henry; Henry et al. 2015), 7 galaxies from GO 11727 and GO 13017 (PI T. Heckman; Heckman et al. 2011; Alexandroff et al. 2015), 2 galaxies from GO 13293 (PI A. Jaskot; Jaskot & Oey 2014), and 5 galaxies from GO 13744 (PI T. Thuan; Izotov et al. 2016). The seven galaxies in T. Heckman's program were originally selected as nearby Lyman-break analogs because of their high FUV luminosity, high UV flux, and compact size. These seven galaxies can also be classified as Green Peas because of their compact sizes in SDSS images and strong [O III]λ5007 emission lines in SDSS spectra. Their sizes and [O III]λ5007 equivalent width are similar to those of the Green Peas in Cardamone et al. (2009). We do not find any obvious bias by including the Lyman-break analogs in the analysis. The seven Green Peas in A. Jaskot's program and T. Thuan's program were selected as LyC leakers because of their extreme [O III]/[O II] ratios. In Figure 1, we show the above samples on the metallicity and dust extinction (Hα/Hβ ratio) diagram. We can see that the current sample is a representative Green Pea sample.

2.2. Properties from SDSS Spectra

From SDSS optical spectra of Green Peas, we get many galactic properties. We use the SDSS pipeline measurements of their Hα, Hβ, [O III]λ5007, and [O II]λ3727 emission-line fluxes and line width. We correct the measured Hα and Hβ fluxes for Milky Way extinction using the attenuation of Schlafly & Finkbeiner (2011; obtained from the NASA/IPAC Galactic Dust Reddening and Extinction tool) and the Fitzpatrick (1999) extinction law. Then, we calculate $E(B-V)$ assuming the Calzetti et al. (2000) extinction law and an intrinsic Hα/Hβ ratio of 2.86 (if Hα/Hβ $<$ 2.86, we set $E(B-V)=0$), and correct the observed emission-line fluxes for dust extinction. We use the stellar mass measured from SDSS spectra by Izotov et al. (2011) for 37 galaxies and the stellar mass in the MPA-JHU SDSS catalog for the other 6 galaxies (all are Lyman-break analogs). Note that the methods used in Izotov et al. (2011) and MPA-JHU are different. The masses here should be treated as very rough estimates because it is very hard to get the masses of the underlying old population for these young starburst galaxies. To measure the metallicity using the T_e method, we measure the [O III]λ4363 line flux in SDSS spectra by fitting a Gaussian function to the continuum-subtracted [O III]λ4363 line spectra. Then, we calculate the metallicity using the [O III]λ4363, [O III]λ5007, and [O II]λ3727 line fluxes following the T_e method described in Izotov et al. (2006) and Ly et al. (2014). We convert the extinction-corrected Hα luminosity to SFR using the formula $\mathrm{SFR}(M_\odot\ \mathrm{yr}^{-1}) = L_{\mathrm{H}\alpha}(\mathrm{erg\ s}^{-1}) \times 10^{-41.27}$ (Kennicutt & Evans 2012). The dust extinction, mass, metallicity, SFR, and emission-line properties of this sample are shown in Tables 1 and 2.

2.3. HST/COS Observation

In our program GO 14201, we used *HST*/COS to observe 20 Green Peas with one orbit per target. First, the targets were imaged in the COS acquisition mode ACQ/IMAGE with MIRRORA, from which we got high-resolution near-UV (NUV) images. The targets were centered accurately (error $\sim$0.″05) on the 2.″5 diameter Primary Science Aperture. Then, the spectra were taken with the grating G160M to cover the rest-frame wavelength ranges of about 1100–1400 Å. The other archival Green Peas in our sample were also observed in the same COS acquisition mode ACQ/IMAGE with MIRRORA, and their spectra were taken with the gratings G130M and/or G160M. The NUV acquisition images of this sample are shown in Figure 2.

The spectral resolution of the above observation is about FWHM $\sim$ 20 km s^{-1} for a point source (James et al. 2014). The actual spectral resolution depends on the source angular sizes. The half-light radius of the NUV emission of Green Peas is about 10 pixels (dispersion $\sim$0.012 Å pixel^{-1}), and it results in FWHM $\sim$ 40 km s^{-1} for the UV continuum spectra. As the Lyα sizes of Green Peas are somewhat larger than the UV continuum sizes (Yang et al. 2017), the spectral resolutions are worse for the Lyα emission lines. We retrieved the COS spectra of this sample from the *HST* MAST archive after they were processed through the standard COS pipeline.

3. Lyα Equivalent Width and Escape Fraction

3.1. Measurements of Lyα Flux, Equivalent Width, and Escape Fraction

Most Green Peas in our sample show strong Lyα emission lines (Figure 3). But about one-third of Green Peas have relatively weak Lyα lines, where the Lyα absorptions in the underlying continuum become non-negligible. Since we want to measure the Lyα emission from the recombination of interstellar H I gas, we need to subtract the underlying continuum.

We first estimate a constant local continuum from wavelength ranges near the Lyα flux where the spectra look flat and there are no obvious emission or absorption features. We calculate the "local continuum" f_λ(continuum) as the average of the spectra in these continuum ranges.

For 33 Green Peas without damped Lyα absorption (see Table 3), we subtract the "local continuum" and calculate the Lyα flux by integrating the spectra in the wavelength range $\sim$1212–1221 Å. Then, we correct the Lyα flux for underlying stellar absorption. The equivalent width of stellar Lyα absorption mostly depends on the star formation history and age of the stellar population (Peña-Guerrero & Leitherer 2013). By comparing the Hα EW of these Green Peas (about 300–900 Å) with model predictions of Hα EW in star-forming galaxies, we found that these Green Peas probably have instantaneous starburst with a burst age of 4–5 Myr (Levesque & Leitherer 2013). According to the model calculations in Peña-Guerrero & Leitherer (2013), the stellar Lyα absorption EW is about -7 Å. So, we correct the Lyα fluxes of these 33 Green Peas with an EW $= -7$ Å absorption.

In another eight Green Peas, the spectra show damped Lyα absorption wings and weak residual Lyα emission lines. The

Table 1
The Sample

ID (1)	R.A. (2)	Decl. (3)	z (4)	$E(B-V)_{\rm MW}$ (5)	$E(B-V)$ (6)	12+log(O/H) (7)	$\log(M/M_{\odot})$ (8)	SFR (9)	R_e (10)	GO# (11)
1333+6246[a]	13:33:03.94	+62:46:03.7	0.31812	0.017	0.000	7.72	8.50	1.4	0.72	13744
1559+0841	15:59:25.97	+08:41:19.1	0.29704	0.033	0.000	8.04	8.97	3.5	0.47	14201
1219+1526	12:19:03.98	+15:26:08.5	0.19560	0.022	0.000	7.81	8.35	13.0	0.33	12928
1514+3852	15:14:08.63	+38:52:07.3	0.33262	0.019	0.000	8.12	9.32	6.4	0.67	14201
1503+3644[a]	15:03:42.82	+36:44:50.8	0.35569	0.013	0.007	8.01	8.22	12.9	0.52	13744
1442−0209[a]	14:42:31.37	−02:09:52.8	0.29367	0.046	0.094	7.95	8.96	21.2	0.50	13744
1133+6514	11:33:03.80	+65:13:41.3	0.24140	0.009	0.040	7.95	9.30	6.4	0.82	12928
1249+1234	12:48:34.64	+12:34:02.9	0.26339	0.026	0.084	8.10	9.05	18.3	0.71	12928
1009+2916	10:09:18.99	+29:16:21.5	0.22192	0.019	0.000	7.92	7.87	3.7	0.46	14201
0815+2156	08:15:52.00	+21:56:23.6	0.14095	0.035	0.014	7.96	8.71	4.4	0.35	13293
1424+4217	14:24:05.73	+42:16:46.3	0.18479	0.009	0.028	8.02	8.34	19.2	0.48	12928
0926+4428	09:26:00.44	+44:27:36.5	0.18069	0.016	0.074	8.02	8.78	14.8	0.43	11727
1152+3400[a]	11:52:04.88	+34:00:49.8	0.34195	0.017	0.114	7.95	8.35	23.2	0.52	13744
0021+0052	00:21:01.02	+00:52:48.1	0.09836	0.021	0.038	8.14	9.30	13.7	0.44	13017
1122+6154	11:22:19.73	+61:54:45.4	0.20456	0.007	0.129	8.14	7.85	6.5	0.32	14201
0925+1403[a]	09:25:32.37	+14:03:13.0	0.30121	0.027	0.134	8.01	8.46	23.8	0.42	13744
0911+1831	09:11:13.34	+18:31:08.2	0.26220	0.024	0.168	7.96	9.75	26.8	0.57	12928
0917+3152	09:17:02.52	+31:52:20.5	0.30036	0.017	0.189	8.10	9.37	21.8	0.47	14201
1137+3524	11:37:22.14	+35:24:26.7	0.19439	0.016	0.043	8.12	9.56	19.5	0.72	12928
1025+3622	10:25:48.38	+36:22:58.4	0.12649	0.010	0.088	8.11	9.20	10.0	0.76	13017
1440+4619	14:40:09.94	+46:19:36.9	0.30076	0.012	0.148	8.13	9.62	38.0	0.72	14201
1429+0643	14:29:47.03	+06:43:34.9	0.17351	0.022	0.053	8.01	9.40	30.6	0.40	13017
1054+5238	10:53:30.83	+52:37:52.9	0.25264	0.013	0.069	8.08	9.77	27.3	0.62	12928
1428+1653	14:28:56.41	+16:53:39.4	0.18164	0.017	0.175	8.12	9.60	22.2	0.77	13017
0303−0759	03:03:21.41	−07:59:23.2	0.16488	0.085	0.000	7.87	9.15	8.9	0.56	12928
1244+0216	12:44:23.37	+02:15:40.4	0.23943	0.021	0.062	8.09	9.65	31.0	1.02	12928
2237+1336	22:37:35.05	+13:36:47.0	0.29350	0.049	0.126	8.11	9.45	30.7	1.08	14201
1454+4528	14:54:35.58	+45:28:56.3	0.26851	0.036	0.169	8.22	9.52	21.4	0.45	14201
1018+4106	10:18:03.24	+41:06:21.0	0.23705	0.012	0.094	7.93	9.32	10.4	0.78	14201
0751+1638	07:51:57.78	+16:38:13.2	0.26471	0.031	0.149	7.85	8.35	7.8	0.80	14201
0822+2241	08:22:47.66	+22:41:44.0	0.21619	0.039	0.195	8.11	8.43	41.6	0.68	14201
1339+1516	13:39:28.30	+15:16:42.1	0.19202	0.026	0.114	8.05	9.43	18.7	0.38	14201
1543+3446	15:43:01.22	+34:46:01.4	0.18733	0.025	0.000	7.96	8.05	2.6	0.77	14201
0938+5428	09:38:13.49	+54:28:25.0	0.10208	0.015	0.123	8.17	9.40	13.6	0.47	11727
0927+1740	09:27:28.67	+17:40:18.6	0.28831	0.026	0.180	8.06	9.26	18.2	0.94	14201
1457+2232	14:57:35.13	+22:32:01.7	0.14861	0.041	0.061	8.02	9.13	11.6	0.42	13293
0749+3337	07:49:36.77	+33:37:16.3	0.27318	0.048	0.203	8.18	9.49	62.3	1.47	14201
1032+2717	10:32:26.95	+27:17:55.2	0.19246	0.018	0.097	8.22	9.65	13.3	0.63	14201
0805+0925	08:05:18.04	+09:25:33.5	0.33034	0.018	0.402	7.98	9.36	22.9	0.81	14201
1205+2620	12:05:00.67	+26:20:47.7	0.34261	0.016	0.178	7.89	9.84	22.0	0.83	14201
0055−0021	00:55:27.46	−00:21:48.7	0.16745	0.022	0.217	8.18	9.70	30.4	0.46	11727
0339−0725	03:39:47.79	−07:25:41.2	0.26071	0.053	0.095	8.31	9.70	29.6	0.88	14201
0747+2336	07:47:58.00	+23:36:32.7	0.15524	0.051	0.085	8.02	9.06	5.9	0.59	14201

Notes. Column descriptions: (1) object ID; (4) redshifts from SDSS optical spectra; (5) Milky Way extinction $E(B-V)_{\rm MW}$, based on Schlafly & Finkbeiner (2011); (6) dust extinction; (7) metallicity; (8) stellar mass; (9) star formation rate in units of $M_{\odot}$ yr^{-1} derived from Hα luminosity; (10) half-light radius in units of kiloparsecs; (11) *HST* programs: GO 14201 (PI S. Malhotra), GO 13744 (PI T. Thuan; Izotov et al. 2016), GO 13293 (PI A. Jaskot; Jaskot & Oey 2014), GO 12928 (PI A. Henry; Henry et al. 2015), and GO 11727 and GO 13017 (PI T. Heckman; Heckman et al. 2011; Alexandroff et al. 2015). These 43 galaxies are sorted by decreasing $f_{\rm esc}^{\rm Ly\alpha}$ from top to bottom.

[a] These are confirmed LyC leakers from Izotov et al. (2016).

(This table is available in its entirety in machine-readable form.)

damped Lyα absorption is caused by interstellar absorption of the continuum and/or the Lyα absorption of the underlying stellar atmosphere continuum spectra. To measure the flux of the residual Lyα emission, we subtract from Lyα line spectra a constant "absorbed continuum." The "absorbed continuum" is estimated as the average location in the wavelength range where the Lyα emission line meets the absorbed continuum. Then, we integrate the Lyα line spectra to get the Lyα flux. Since the above absorption correction already includes stellar Lyα absorption, we do not need to correct the stellar absorption for these eight Green Peas. Note that in some cases the stellar absorption might have a very narrow component that is not fully corrected by this method.

In the remaining two Green Peas (GP0339−0725 and GP0747+2336), the Lyα lines are too weak and we did not detect Lyα emission.

Then, we correct the measured Lyα fluxes for Milky Way extinction using the Fitzpatrick (1999) extinction law. The rest-frame EW(Lyα) is calculated using the Lyα fluxes and the "local continuum" as EW(Lyα) = flux(Lyα)/f_{λ}(continuum)/

Table 2
Line Measurements from SDSS Spectra

ID (1)	[O II]3727 (2)	[O III]4363 (3)	Hβ (4)	[O III]4959 (5)	[O III]5007 (6)	Hα (7)	EW(Hα) (8)	[O III]/[O II] (9)
1333+6246	115 ± 5	13.6 ± 2.7	58 ± 4	129 ± 2	390 ± 6	78 ± 4	538	4.5
1559+0841	169 ± 4	9.4 ± 1.3	124 ± 12	229 ± 2	693 ± 6	232 ± 11	288	5.5
1219+1526	467 ± 8	108.8 ± 4.9	776 ± 9	1635 ± 8	4953 ± 25	2207 ± 18	744	14.2
1514+3852	270 ± 5	9.2 ± 3.1	139 ± 3	248 ± 2	751 ± 6	327 ± 6	232	3.7
1503+3644	220 ± 3	19.3 ± 1.6	184 ± 2	397 ± 2	1203 ± 7	534 ± 21	921	7.1
1442−0209	248 ± 5	32.2 ± 2.4	299 ± 4	647 ± 5	1960 ± 14	988 ± 13	858	9.0
1133+6514	268 ± 5	19.2 ± 2.3	196 ± 3	376 ± 2	1138 ± 7	592 ± 6	263	5.3
1249+1234	575 ± 8	28.8 ± 2.4	364 ± 5	740 ± 5	2242 ± 14	1169 ± 12	717	4.6
1009+2916	139 ± 4	22.0 ± 2.3	173 ± 4	382 ± 3	1156 ± 9	473 ± 16	422	11.1
0815+2156	293 ± 5	56.4 ± 3.3	462 ± 5	1065 ± 7	3227 ± 22	1383 ± 13	717	14.0
1424+4217	1129 ± 16	114.9 ± 3.6	1119 ± 11	2463 ± 11	7459 ± 33	3333 ± 25	629	8.4
0926+4428	1090 ± 14	56.3 ± 3.5	733 ± 8	1318 ± 7	3994 ± 22	2314 ± 18	437	4.4
1152+3400	237 ± 4	22.5 ± 1.3	228 ± 3	461 ± 2	1397 ± 7	756 ± 5	497	6.7
0021+0052	5172 ± 29	127.8 ± 6.7	2909 ± 14	4275 ± 12	12949 ± 36	8855 ± 32	320	3.1
1122+6154	257 ± 5	11.6 ± 1.3	200 ± 4	369 ± 3	1118 ± 10	667 ± 10	495	4.9
0925+1403	297 ± 7	25.8 ± 4.0	282 ± 4	596 ± 4	1806 ± 11	960 ± 10	633	6.7
0911+1831	576 ± 10	15.5 ± 3.2	379 ± 5	442 ± 3	1340 ± 9	1343 ± 14	348	2.5
0917+3152	300 ± 5	6.2 ± 2.3	210 ± 3	244 ± 1	739 ± 4	760 ± 7	250	2.5
1137+3524	1519 ± 17	51.1 ± 2.7	941 ± 10	1563 ± 7	4733 ± 21	2865 ± 21	434	3.9
1025+3622	1816 ± 17	60.7 ± 4.5	1038 ± 10	1746 ± 10	5289 ± 31	3318 ± 25	312	3.4
1440+4619	895 ± 11	19.5 ± 3.0	441 ± 5	637 ± 4	1929 ± 12	1513 ± 14	325	2.4
1429+0643	2245 ± 23	152.3 ± 6.8	1785 ± 15	3503 ± 15	10610 ± 46	5524 ± 37	686	5.8
1054+5238	1068 ± 13	32.5 ± 3.3	661 ± 7	982 ± 6	2974 ± 17	2068 ± 16	304	3.4
1428+1653	1574 ± 17	19.6 ± 3.0	706 ± 8	733 ± 4	2220 ± 13	2511 ± 20	261	1.5
0303−0759	488 ± 8	74.0 ± 2.5	656 ± 7	1301 ± 8	3941 ± 23	1963 ± 18	608	10.3
1244+0216	1252 ± 12	64.1 ± 3.3	853 ± 7	1681 ± 8	5091 ± 25	2665 ± 18	667	4.9
2237+1336	733 ± 9	19.3 ± 2.7	376 ± 4	587 ± 4	1780 ± 11	1291 ± 12	353	2.6
1454+4528	498 ± 8	9.2 ± 3.2	293 ± 4	401 ± 3	1215 ± 8	1033 ± 11	277	2.6
1018+4106	292 ± 5	28.5 ± 1.9	263 ± 3	539 ± 3	1633 ± 10	846 ± 8	570	6.5
0751+1638	216 ± 6	10.7 ± 3.6	115 ± 3	187 ± 2	567 ± 5	401 ± 7	299	2.8
0822+2241	1063 ± 11	54.0 ± 3.1	781 ± 6	1551 ± 6	4699 ± 19	2886 ± 17	605	4.4
1339+1516	602 ± 8	61.4 ± 3.2	667 ± 7	1485 ± 6	4499 ± 18	2222 ± 57	523	8.4
1543+3446	185 ± 6	15.4 ± 2.3	194 ± 5	343 ± 4	1037 ± 11	480 ± 7	342	7.5
0339−0725	978 ± 12	14.7 ± 2.3	538 ± 6	733 ± 4	2220 ± 13	1786 ± 15	345	2.6
0938+5428	3305 ± 28	67.9 ± 4.0	1887 ± 15	2627 ± 13	7957 ± 39	6313 ± 39	353	2.7
0927+1740	328 ± 6	17.7 ± 2.1	196 ± 4	419 ± 3	1268 ± 9	707 ± 9	707	4.0
1457+2232	764 ± 9	103.1 ± 2.7	868 ± 12	2096 ± 12	6349 ± 36	2758 ± 20	707	9.9
0749+3337	1312 ± 14	20.3 ± 2.4	652 ± 7	811 ± 5	2457 ± 14	2447 ± 27	361	1.9
1032+2717	845 ± 8	25.1 ± 0.8	520 ± 5	910 ± 4	2757 ± 13	1687 ± 13	651	3.8
0805+0925	73 ± 5	4.3 ± 3.5	72 ± 4	123 ± 3	371 ± 8	333 ± 6	353	4.0
1205+2620	324 ± 5	9.0 ± 3.7	165 ± 3	198 ± 1	599 ± 4	587 ± 8	350	1.9
0055−0021	1738 ± 11	29.0 ± 3.0	956 ± 5	1197 ± 3	3626 ± 10	3587 ± 12	249	2.1
0747+2336	363 ± 5	35.8 ± 1.8	354 ± 5	796 ± 5	2411 ± 16	1166 ± 11	366	7.6

Note. Observed line fluxes from SDSS spectra in units of 10^{-17} erg s^{-1} cm^{-2}. The EW(Hα) is the rest-frame Hα equivalent width. The [O III]/[O II] ratios are extinction corrected using the Calzetti et al. (2000) extinction law.

(This table is available in its entirety in machine-readable form.)

(1+redshift). The Lyα escape fraction, $f_{\rm esc}^{\rm Ly\alpha}$, is defined as the ratio of the measured Lyα flux to the intrinsic Lyα flux. Assuming case-B recombination, the intrinsic Lyα flux is about 8.7 times the dust extinction-corrected Hα flux (see Henry et al. 2015 for discussions about the factor 8.7). Thus, $f_{\rm esc}^{\rm Ly\alpha}$ is Lyα (observed)/(8.7 × $\rm H\alpha_{corrected}$). The SDSS Hα spectra were taken with a 3″ diameter aperture that matches the COS 2.″5 diameter aperture very well. Note that many Lyα galaxies have a very extended Lyα halo (e.g., Östlin et al. 2009; Hayes et al. 2013; Momose et al. 2014). For these Green Pea galaxies, their Lyα to UV size ratios are about 2–4 (Yang et al. 2017). Thus, the COS 2.″5 aperture probably captured the majority of Lyα emission of those Green Peas.

Because the total counts per pixel in the UV continuum of this sample are small, we calculate the error spectra using the Poisson noise of the total counts. The statistical errors of the Lyα fluxes are calculated from the error spectra using the error propagation formula. The Lyα flux, luminosity, EW(Lyα), and $f_{\rm esc}^{\rm Ly\alpha}$ are shown in Table 3. A comparison of $f_{\rm esc}^{\rm Ly\alpha}$ and EW(Lyα) is shown in Figure 4.

3.2. Lyα EW Distribution of Green Peas

With a large sample of Green Peas that covers the whole ranges of dust and metallicity, we now have a more reliable estimation of the EW(Lyα) distribution of Green Peas than previous results. Forty-one out of the forty-three Green Peas

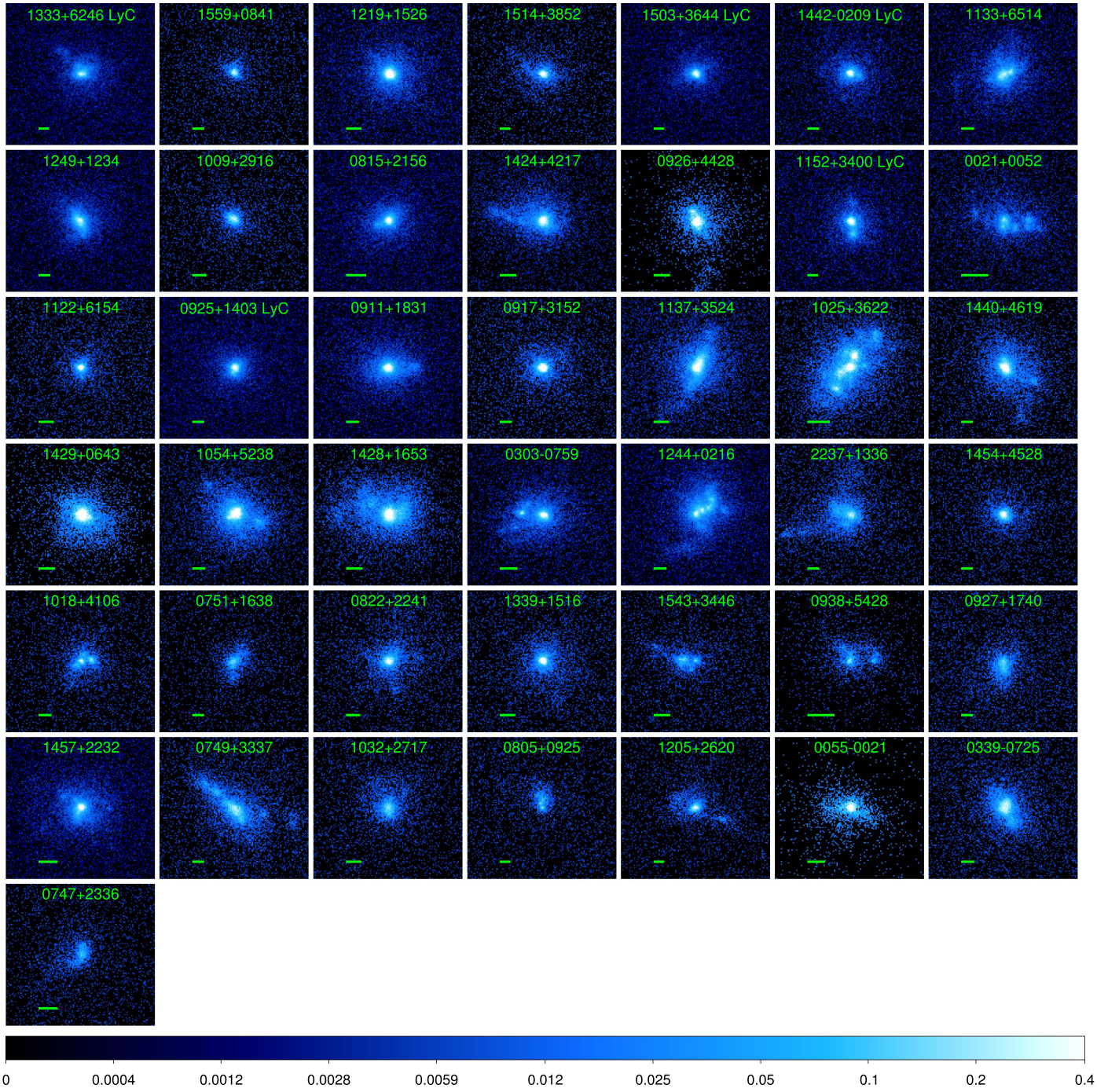

Figure 2. $3'' \times 3''$ NUV images of Green Peas from the COS target acquisitions. In all panels, the colors are in log-scale with the same count-rate limits (from 0 to 0.4). These images are sorted by decreasing $f_{\rm esc}^{\rm Ly\alpha}$ from left to right, and from top to bottom. The label shows the ID of each Green Pea. The five LyC leakers are marked with "LyC." The green bar in each panel shows the physical scale of 1 kpc.

show Lyα emission lines. Twenty-eight out of the forty-three GPs (65%) in our sample have rest-frame EW(Lyα) $\gtrsim$ 20 Å and would be classified as LAEs in a typical high-redshift narrowband survey. We compared the EW(Lyα) distribution of these 28 Green Peas to that high-redshift LAE samples. The high-redshift LAE samples include a sample of $z = 2.8$ narrowband-selected LAEs (Zheng et al. 2016) and a sample of spectroscopically confirmed LAEs at $z = 5.7$ or 6.5 (Kashikawa et al. 2011). To be consistent with the methods used in high-z LAEs studies, we use the EW(Lyα) of Green Peas without correcting for stellar Lyα absorption. We also add a *GALEX*-selected $z \sim 0.3$ LAE sample to the comparison (Deharveng et al. 2008; Finkelstein et al. 2009; Scarlata et al. 2009; Cowie et al. 2011). Figure 5 shows the cumulative EW(Lyα) fraction distributions of these four samples. These 28 Green Peas have EW(Lyα) distributions very similar to the high-redshift ($z = 2.8$) sample. So, Green Peas in general are the best nearby analogs of high-z LAEs.

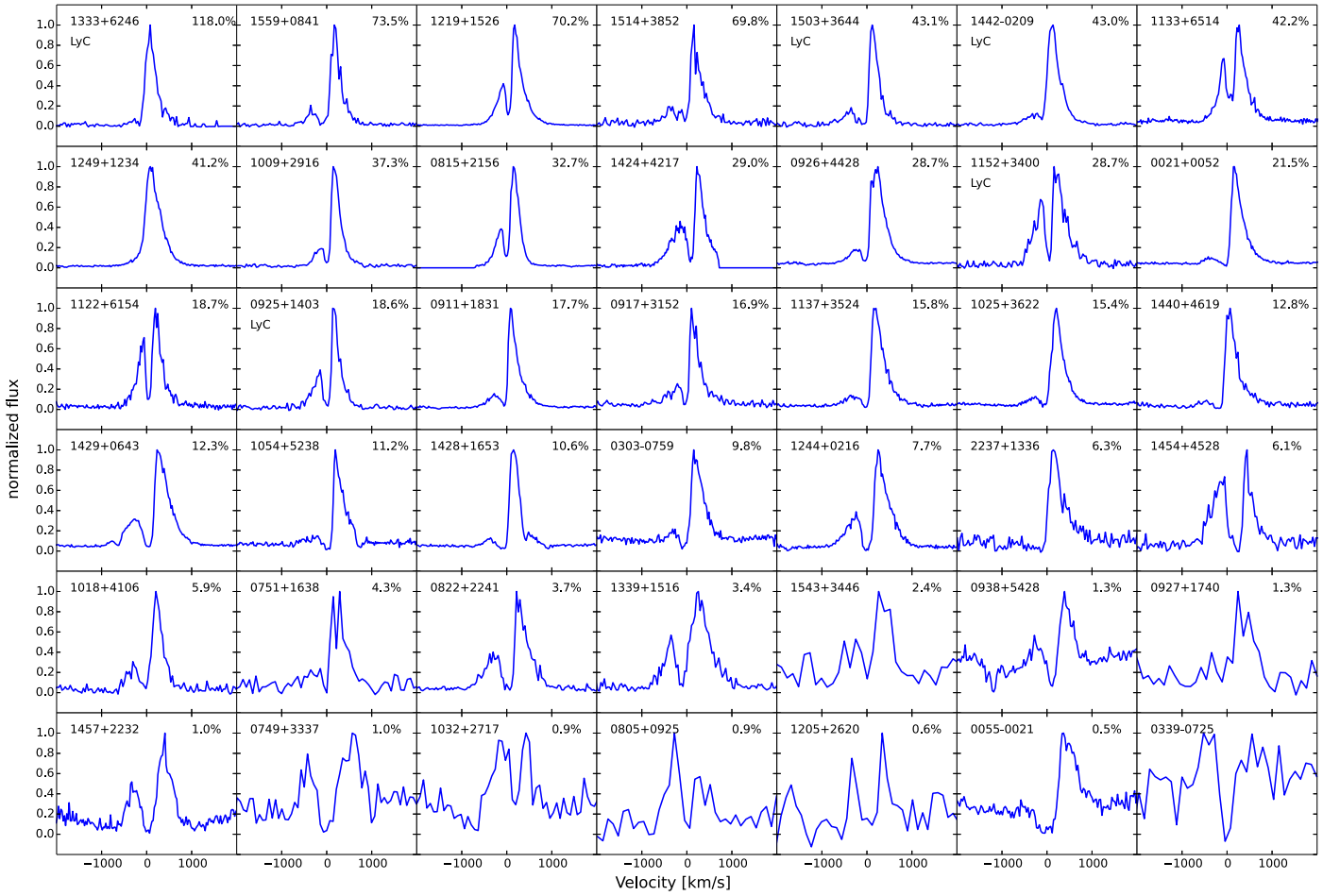

Figure 3. Lyα emission-line spectra of Green Peas before subtracting the continuum. These 42 galaxies are sorted by decreasing $f_{\rm esc}^{\rm Ly\alpha}$ from left to right, and from top to bottom. The ID and $f_{\rm esc}^{\rm Ly\alpha}$ are given in each panel. The five LyC leakers are marked with "LyC." The last galaxy (GP0339−0725) shows weak Lyα absorption. One Green Pea (GP0747+2336) is not shown here, because its Lyα spectra is very noisy, and no Lyα emission or absorption lines are detected.

4. Lyα Escape and Lyα Profiles

4.1. Kinematic Features of Lyα Profile

In the Lyα escape process, Lyα photons are resonant scattered by the H I gas. Depending on the column density and bulk motion of H I gas, the resonant scatterings can significantly modify the Lyα profile. Therefore, the Lya profile carries a lot of information about the H I gas properties. High-z LAEs usually show an asymmetric or a double-peaked Lyα emission-line profile (e.g., Rhoads et al. 2003; Kashikawa et al. 2011; Erb et al. 2014). For LAEs with detected optical emission lines and systemic redshifts, the peaks of Lyα profiles are usually redshifted with respect to the systemic velocities (McLinden et al. 2011, 2014; Chonis et al. 2013; Hashimoto et al. 2013; Erb et al. 2014; Shibuya et al. 2014; Song et al. 2014). The velocity offset of the Lyα emission line from the systemic velocity is usually smaller in LAEs than in continuum-selected galaxies with weaker Lyα emission lines or Lyα absorptions (Shapley et al. 2003).

Most Green Peas show double-peaked Lyα profiles (Figure 3). For a typical double-peaked profile, we define the "red peak" as the peak in the Lyα line profile occurring at velocity >0, the "blue peak" as the Lyα peak at velocity <0, and the "valley" as the flux minimum between the two peaks.

With a sample covering a large range of properties, we can see that the Lyα profiles are diverse. In Figure 3, the 42 Green Peas are sorted by decreasing $f_{\rm esc}^{\rm Ly\alpha}$ from top left to bottom right. Three Green Peas with high $f_{\rm esc}^{\rm Ly\alpha}$ show single-peak profiles where the peak velocities are close to zero (GP1333+6246, GP1442−0209, and GP1249+1234). Many Green Peas with intermediate $f_{\rm esc}^{\rm Ly\alpha}$ generally show double-peaked profiles with much stronger red peaks than blue peaks. On the other hand, many Green Peas with low $f_{\rm esc}^{\rm Ly\alpha}$ have a relatively large ratio of blue peak to red peak.

As in Paper I, we measure four kinematic features of the Lyα profile: (i) the blue peak velocity V(blue-peak), (ii) the red peak velocity V(red-peak), (iii) the peak separation V(red-peak) $-V$(blue-peak), and (iv) the FWHM of the red portion of the Lyα profile, FWHM(red). The velocities are relative to the systemic redshift derived from SDSS spectra. The measurements of these kinematic features are shown in Table 3. For some Green Peas, we do not measure their velocities because their Lyα profiles are too noisy. In the notes to Table 3, we explain the reason for each profile without a velocity measurement. To measure the errors of the velocity peaks, we use a Monte Carlo method to generate 1000 fake spectra by adding Gaussian noise (with the error spectra as the σ of the Gaussian noise) to the observed spectra. Then, we measure the peak velocities of these 1000 fake spectra and use the standard deviations as the errors. In summary, we have measurements of V(blue-peak) and the peak separation in 28 galaxies, and of V (red-peak) and FWHM(red) in 37 galaxies.

Table 3
Lyα Properties

ID	Lyα Flux (10^{-16} erg s^{-1} cm^{-2})	log(L(Lyα) erg s^{-1})	EW(Lyα) (Å)	$f_{esc}^{Ly\alpha}$	V(Blue-peak) (km s^{-1})	V(Red-peak) (km s^{-1})	FWHM(Red) (km s^{-1})
(1)	(2)	(3)	(4)	(5)	(6)	(7)	(8)
1333+6246[a]	160.4 ± 2.8	42.7	72.3	1.180	…[b]	79 ± 17	245 ± 24
1559+0841	145.0 ± 3.1	42.6	96.0	0.735	−355 ± 24	168 ± 17	188 ± 29
1219+1526	1345.3 ± 5.9	43.2	164.5	0.702	−76 ± 13	176 ± 13	213 ± 18
1514+3852	180.8 ± 4.1	42.8	60.0	0.698	…[c]	159 ± 17	222 ± 58
1503+3644[a]	195.2 ± 4.3	42.9	106.6	0.431	−349 ± 43	118 ± 23	229 ± 27
1442−0209[a]	504.5 ± 5.6	43.1	134.9	0.430	…[b]	135 ± 26	267 ± 25
1133+6514	208.0 ± 1.9	42.6	42.3	0.422	−69 ± 15	271 ± 22	234 ± 21
1249+1234	528.0 ± 2.6	43.1	101.8	0.412	…[b]	83 ± 27	364 ± 17
1009+2916	142.8 ± 2.5	42.3	69.5	0.373	−116 ± 45	144 ± 22	206 ± 26
0815+2156	401.2 ± 1.4	42.3	82.2	0.327	−121 ± 13	144 ± 13	216 ± 19
1424+4217	858.6 ± 4.1	42.9	89.5	0.290	−150 ± 32	224 ± 10	208 ± 16
0926+4428	636.8 ± 2.3	42.8	47.8	0.287	−165 ± 51	244 ± 17	327 ± 18
1152+3400[a]	248.6 ± 4.6	43.0	74.5	0.287	−146 ± 26	158 ± 44	235 ± 30
0021+0052	1523.5 ± 9.7	42.6	32.8	0.215	−418 ± 38	164 ± 12	253 ± 16
1122+6154	144.1 ± 2.1	42.2	60.0	0.187	−56 ± 21	194 ± 26	202 ± 25
0925+1403[a]	225.1 ± 4.1	42.8	90.0	0.186	−145 ± 24	133 ± 23	160 ± 25
0911+1831	315.7 ± 2.1	42.8	56.5	0.177	−278 ± 17	81 ± 12	207 ± 17
0917+3152	167.7 ± 3.3	42.7	38.0	0.169	−209 ± 42	104 ± 22	189 ± 25
1137+3524	381.1 ± 3.4	42.6	40.4	0.158	−355 ± 46	201 ± 22	285 ± 20
1025+3622	436.6 ± 3.6	42.3	26.3	0.154	−248 ± 39	210 ± 12	253 ± 15
1440+4619	214.2 ± 3.6	42.8	33.8	0.128	…[b]	67 ± 29	248 ± 30
1429+0643	607.1 ± 2.9	42.7	42.7	0.123	−257 ± 34	231 ± 19	324 ± 19
1054+5238	153.5 ± 2.6	42.5	17.7	0.112	−314 ± 88	192 ± 12	225 ± 25
1428+1653	311.9 ± 2.2	42.5	29.1	0.106	−360 ± 25	150 ± 20	242 ± 18
0303−0759	99.6 ± 2.1	41.9	14.2	0.098	−313 ± 48	153 ± 26	270 ± 23
1244+0216	189.9 ± 1.6	42.5	47.0	0.077	−240 ± 14	247 ± 14	302 ± 25
2237+1336	51.4 ± 2.6	42.1	15.3	0.063	…[b]	141 ± 36	272 ± 35
1454+4528	72.3 ± 2.1	42.2	30.0	0.061	−56 ± 58	444 ± 18	202 ± 47
1018+4106	47.0 ± 1.5	41.9	33.1	0.059	−306 ± 44	206 ± 25	238 ± 32
0751+1638	13.9 ± 1.3	41.5	15.8	0.043	…[c]	…[c]	…[c]
0822+2241	156.5 ± 2.9	42.3	51.6	0.037	−304 ± 65	217 ± 31	262 ± 39
1339+1516	82.5 ± 1.9	41.9	44.7	0.034	−351 ± 30	256 ± 42	435 ± 62
1543+3446[d]	10.6 ± 0.8	41.0	5.4	0.024	…[c]	261 ± 94	407 ± 90
0938+5428[d]	107.1 ± 2.0	41.5	3.5	0.013	−279 ± 20	390 ± 17	333 ± 43
0927+1740[d]	14.0 ± 1.1	41.6	7.2	0.013	…[c]	242 ± 91	408 ± 150
1457+2232[d]	32.3 ± 0.6	41.3	5.3	0.010	−329 ± 37	406 ± 14	321 ± 54
0749+3337	9.2 ± 1.7	41.3	8.9	0.010	−427 ± 72	568 ± 72	405 ± 114
1032+2717[d]	19.2 ± 0.9	41.3	5.5	0.009	…[c]	…[c]	…[c]
0805+0925[d]	9.5 ± 1.3	41.5	9.2	0.009	…[c]	…[c]	…[c]
1205+2620[d]	5.8 ± 1.3	41.4	3.0	0.006	…[c]	…[c]	…[c]
0055−0021[d]	31.3 ± 1.0	41.4	3.2	0.005	…[c]	368 ± 45	420 ± 39
0339−0725[e]	−1.4 ± 1.8	…	…	…	…	…	…
0747+2336[e]	…	…	…	…	…	…	…

Notes. Column descriptions: (1) object ID; (2) Lyα emission-line flux; (3) Lyα emission-line luminosity; (4) equivalent width of the Lyα line; (5) Lyα escape fraction; (6) velocity of the Lyα blue peak; (7) velocity of the Lyα red peak; (8) FWHM of the red portion of the Lyα profile. These 43 galaxies are sorted by decreasing $f_{esc}^{Ly\alpha}$ from top to bottom.

[a] These are confirmed LyC leakers from Izotov et al. (2016).

[b] Their Lyα profiles do not have blue peaks.

[c] Their Lyα profiles are too noisy for measuring Lyα kinematic features.

[d] These Green Peas show damped Lyα absorption wings in their Lyα spectra.

[e] No Lyα emission line was detected.

(This table is available in its entirety in machine-readable form.)

4.2. Relations between Lyα Escape and Lyα Kinematics

We show the relations between $f_{esc}^{Ly\alpha}$ and the kinematic features of Lyα profiles in Figure 6. As $f_{esc}^{Ly\alpha}$ covers a range of about 3 dex, we show it in logarithmic scale. $f_{esc}^{Ly\alpha}$ shows anti-correlations with all four kinematic features—V(blue-peak), V(red-peak), the peak separation V(red-peak)−V(blue-peak), and the FWHM(red). We calculate the Spearman correlation coefficients of these relations (shown in each panel of Figure 6).

In Paper I, we found that $f_{esc}^{Ly\alpha}$ correlates strongly with V(blue-peak). Here we can see most Green Peas still follow the correlation, but there are a few Green Peas with large scatter. So, the overall correlation is worse than in Paper I. These

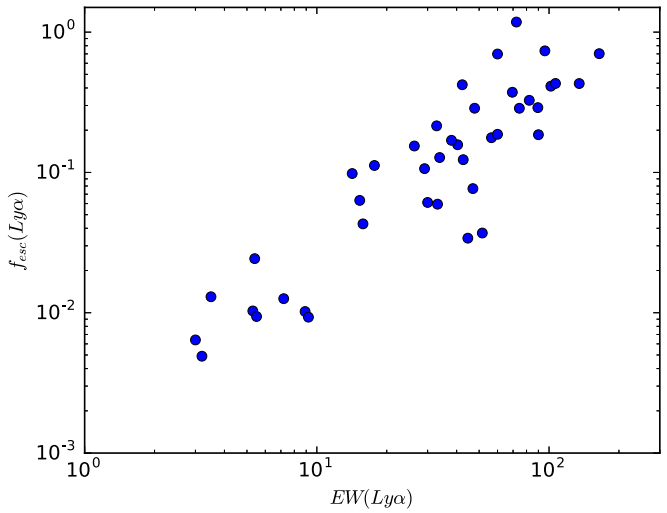

Figure 4. Comparison of the $f_{\rm esc}^{\rm Ly\alpha}$ and EW(Lyα) of the Green Peas.

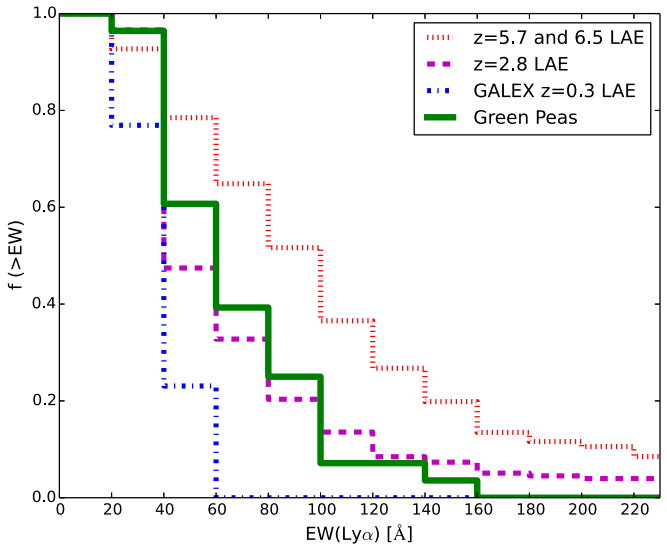

Figure 5. Here we compare the rest-frame EW(Lyα) distribution of Green Peas with different samples. The solid green line shows the sample of 28 Green Peas with EW(Lyα) $\gtrsim$ 20 Å. The blue dashed–dotted line shows the *GALEX* $z \sim 0.3$ LAE sample (Finkelstein et al. 2009; Scarlata et al. 2009; Cowie et al. 2011). The magenta dashed line shows the $z = 2.8$ LAE sample from Zheng et al. (2016). The red dotted line shows the $z = 5.7$ and 6.5 LAE sample from Kashikawa et al. (2011).

outliers suggest that the Lyα blue peak velocities are determined by multiple mechanisms. For example, one outlier (GP1454+4528, marked with a square and different color in Figure 6) has a distinct profile with the largest positive V(valley) (the velocity at the inter-peaks dip) and very strong blue portion Lyα emission. Its V(blue-peak) and V(red-peak) are clearly offset from the trends. However, if we exchange V(blue-peak) and V(red-peak), then it follows the trends very well. There are probably strong gas inflows as well as gas outflows in this galaxy. We excluded this object from the calculation of the correlation coefficients.

On the other hand, in Paper I, we found a large scatter between $f_{\rm esc}^{\rm Ly\alpha}$ and V(red-peak) with 12 Green Peas. However, as the current sample covers a large range of $f_{\rm esc}^{\rm Ly\alpha}$ and V(red-peak), $f_{\rm esc}^{\rm Ly\alpha}$ shows an anti-correlation with V(red-peak). The relation between $f_{\rm esc}^{\rm Ly\alpha}$ and V(red-peak) in this Green Peas sample is very

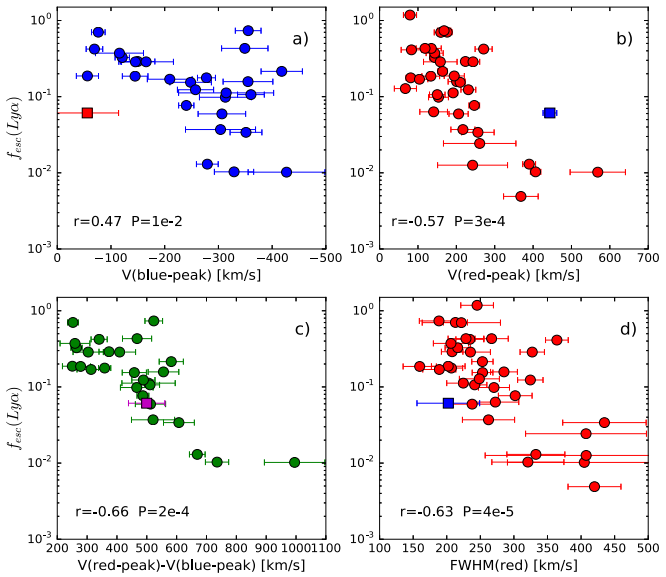

Figure 6. Relations between $f_{\rm esc}^{\rm Ly\alpha}$ and the kinematic features of the Lyα profile: (a) $f_{\rm esc}^{\rm Ly\alpha}$ and the blue peak velocity of Lyα profile, V(blue-peak); (b) $f_{\rm esc}^{\rm Ly\alpha}$ and the red peak velocity of Lyα profile, V(red-peak); (c) $f_{\rm esc}^{\rm Ly\alpha}$ and the peak separation of Lyα profile; and (d) $f_{\rm esc}^{\rm Ly\alpha}$ and the FWHM of the red portion of Lyα profile, FWHM(red). The Spearman correlation coefficient and null probability are shown. GP1454+4528 with possible gas inflows is marked by a square in different color in each panel.

similar to the relations between EW(Lyα) and V(red-peak) in high-redshift LAEs and LBGs, where the LAEs have high EW(Lyα) and small V(red-peak), while the LBGs have small EW(Lyα) and large V(red-peak) (Shapley et al. 2003; Hashimoto et al. 2013; Erb et al. 2014).

We also found that $f_{\rm esc}^{\rm Ly\alpha}$ anti-correlates with FWHM(red). We perform a linear fit to this relation and obtain the following function:

$$\log(f_{\rm esc}^{\rm Ly\alpha}) = -0.545 \times (\mathrm{FWHM(red)}/100\ \mathrm{km\ s^{-1}}) + 0.563.$$

The scatter of this relation is 0.43 dex in $\log(f_{\rm esc}^{\rm Ly\alpha})$. Since any high-$z$ LAE with a spectrum will have a measured FWHM for the red peak, it is easy to use this relation to infer the Lyα escape fraction of high-z LAEs.

Brief interpretations. The Lyα profile depends on the column density and the kinematics of H I gas. As the H I column density increases, the number of scatterings of Lyα photons increase. More scatterings generally result in larger offsets of peak velocities (V(blue-peak) and V(red-peak)) and broader line profiles (FWHM(red)). Also, more scatterings increase the Lyα photons' path lengths, which makes the Lyα radiation more susceptible to dust extinction and consequently decreases the Lyα escape fraction. Thus, those anti-correlations mostly indicate that the $f_{\rm esc}^{\rm Ly\alpha}$ decreases as the column density of the H I gas increases.

5. Lyα Escape and Other Galactic Properties

5.1. Dust Extinction, Stellar Mass, and Metallicity

These Green Peas are very well-studied galaxies and provide a great opportunity to explore the dependence of Lyα escape on other galactic properties. Previous studies have found that $f_{\rm esc}^{\rm Ly\alpha}$ anti-correlates with dust extinction (Atek et al. 2014; Cowie et al. 2011; Paper I). However, the relation between $f_{\rm esc}^{\rm Ly\alpha}$ and metallicity is unclear (Finkelstein et al. 2011;

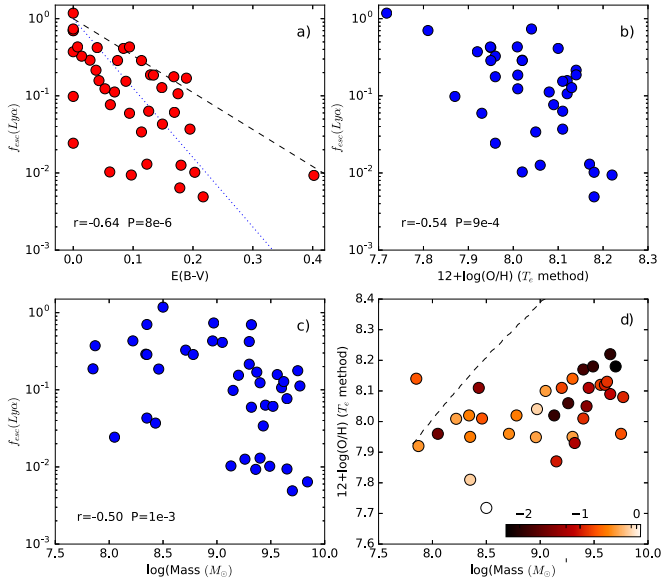

Figure 7. (a) Relation between $f_{\rm esc}^{{\rm Ly}\alpha}$ and dust extinction $E(B-V)$. The black dashed (blue dotted) line shows the expected Lyα escape fraction if Lyα is only absorbed by dust following the Calzetti et al. (2000) extinction law (the SMC extinction law). (b) Relation between $f_{\rm esc}^{{\rm Ly}\alpha}$ and the metallicity from the T_e method. (c) Relation between $f_{\rm esc}^{{\rm Ly}\alpha}$ and stellar mass. The Spearman correlation coefficient and null probability are shown in panels (a)–(c). (d) The mass–metallicity relation of this sample. The color bar shows the value of $\log(f_{\rm esc}^{{\rm Ly}\alpha})$. The dashed line shows the mass–metallicity relation for SDSS galaxies in Amorín et al. (2010).

Atek et al. 2014; Hayes et al. 2014; Paper I). Our sample covers the full ranges of dust extinction and metallicity of Green Peas. In Figure 7, we show the relations between $f_{\rm esc}^{{\rm Ly}\alpha}$ and $E(B-V)$, metallicity, and stellar mass. The Spearman correlation coefficients of these relations are shown Figure 7.

Green Peas with higher dust extinction tend to have smaller $f_{\rm esc}^{{\rm Ly}\alpha}$, confirming that dust extinction is an important factor in Lyα escape. In Figure 7(a), we also show the expected Lyα escape fractions if Lyα is only absorbed by dust following the Calzetti et al. (2000) extinction law (dashed line) or the SMC extinction law (Gordon et al. 2003; dotted line). The SMC extinction law is steeper in FUV than the Calzetti et al. (2000) extinction law, so the extinction of Lyα emission is larger for the SMC extinction law. Many Green Peas are below the dashed and dotted lines, because resonant scatterings increase the escape path length of Lyα photons and the chances of being absorbed by dust. Interestingly, many Green Peas are above the relation for the SMC extinction law. If the dust extinction in Green Peas follows the SMC extinction law, then it probably suggests that resonant scatterings in clumpy dust distributions *decrease* the dust extinction of Lyα emission (Neufeld 1990; Hansen & Oh 2006; Finkelstein et al. 2009; Scarlata et al. 2009; but also see Laursen et al. 2013 showing that clumpy media does not decrease the dust extinction of Lyα for typical conditions in LAEs).

$f_{\rm esc}^{{\rm Ly}\alpha}$ also anti-correlates with metallicity and stellar mass. In the $f_{\rm esc}^{{\rm Ly}\alpha}$ versus metallicity diagram, only 37 galaxies with [O III]λ4363 line S/N >3 are shown. In Figure 7, we also show the mass–metallicity relation of Green Peas and color the sample with $f_{\rm esc}^{{\rm Ly}\alpha}$. The dashed line shows the mass–metallicity relation for SDSS galaxies in Amorín et al. (2010), where the metallicity of SDSS galaxies is calculated using the same

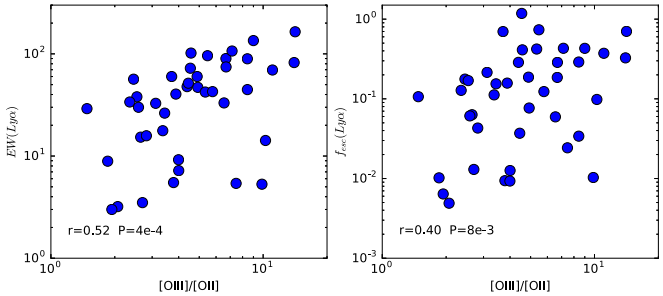

Figure 8. Left: relation between EW(Lyα) and [O III]/[O II]. Right: relation between $f_{\rm esc}^{{\rm Ly}\alpha}$ and [O III]/[O II]. [O III]/[O II] is defined as ([O III]λ4959 +[O III]λ5007)/([O II]λ3726+[O II]λ3729). The Spearman correlation coefficient and null probability are shown in each panel.

effective temperature method. These Green Peas have lower metallicities than the mass−metallicity relation of SDSS galaxies, similar to other emission-line-selected galaxies (Xia et al. 2012; Ly et al. 2014; Song et al. 2014). These Green Peas with lower metallicities and smaller masses have less dust extinction. In addition, ionized gas outflows can blow out the metal-enriched gas and decrease the metallicity and dust extinction. At the same time, the ionized gas outflows can make holes with low H I column densities and help Lyα escape.

5.2. Morphology and Size of UV Emission

We get the NUV image of each object from the COS target acquisition (Figure 2). So, we also explore the relation between Lyα escape and the UV morphology. The pixel scale of the NUV image is 0.0235 ± 0.0001 arcsec pixel^{-1}. The FWHM of the point-spread function is about 2 pixels or $0\farcs047$. As we can see from the images, most Green Peas are very small and compact. Multiple clumps, tidal tails, and asymmetric shapes are common, which may suggest that dwarf–dwarfmergers are common in Green Peas. In Figure 2, these images are sorted by decreasing $f_{\rm esc}^{{\rm Ly}\alpha}$ from left to right, and from top to bottom. $f_{\rm esc}^{{\rm Ly}\alpha}$ does not show an obvious relation with the morphology.

We then use GALFIT (Peng et al. 2010) to measure the galaxy size. We fit the image with a single Sérsic profile component and get the half-light radius of each galaxy. The half-light radii are shown in Table 1. The relation between $f_{\rm esc}^{{\rm Ly}\alpha}$ and the half-light radius has very large scatter.

5.3. [O III]/[O II] Ratio

Green Peas are selected to have large [O III]/[O II] ratios. The [O III]/[O II] ratio has been used to select LyC leaker candidates, and a large [O III]/[O II] may indicate the existence of paths with low H I optical depth (Jaskot & Oey 2014; Izotov et al. 2016). In Figure 8, we show the EW(Lyα) versus [O III]/[O II] and $f_{\rm esc}^{{\rm Ly}\alpha}$ versus [O III]/[O II] relations. The Lyα line strength generally increases with [O III]/[O II], but the scatter is large.

6. Lyα Profile Fitting

The Lyα emission-line profiles can usually be explained by resonant scatterings of Lyα photons by an outflowing H I gas shell (e.g., Ahn et al. 2001; Dijkstra et al. 2006; Verhamme et al. 2006; Schaerer et al. 2011). To extract more information from the Lyα profiles and explore the physical process of Lyα escape, we fit the Lyα profiles with the outflowing H I shell radiative transfer model (Dijkstra 2014; Gronke et al. 2015).

Table 4
Lyα Profile Model Parameters

ID	$\log(N_{\rm H\,I}\ {\rm cm}^{-2})$	$V_{\rm exp}$ (km s^{-1})	$\log(T)$ (K)	τ_d	σ (km s^{-1})
(1)	(2)	(3)	(4)	(5)	(6)
1333+6246	$19.39^{+0.08}_{-0.07}$	270^{+4}_{-4}	$5.0^{+0.2}_{-0.1}$	$0.71^{+0.09}_{-0.08}$	125^{+2}_{-2}
1559+0841	$19.40^{+0.07}_{-0.07}$	90^{+3}_{-4}	$3.0^{+0.1}_{-0.1}$	$0.64^{+0.08}_{-0.06}$	203^{+2}_{-2}
1514+3852	$19.20^{+0.07}_{-0.07}$	80^{+4}_{-3}	$3.8^{+0.1}_{-0.1}$	$0.01^{+0.01}_{-0.00}$	305^{+7}_{-7}
1503+3644	$16.81^{+0.08}_{-0.08}$	140^{+4}_{-4}	$5.4^{+0.2}_{-0.1}$	$0.14^{+0.07}_{-0.05}$	266^{+5}_{-5}
1442−0209	$18.80^{+0.07}_{-0.07}$	150^{+4}_{-4}	$4.2^{+0.2}_{-0.2}$	$0.01^{+0.01}_{-0.00}$	230^{+2}_{-2}
1009+2916	$19.60^{+0.07}_{-0.07}$	30^{+4}_{-4}	$3.4^{+0.1}_{-0.1}$	$0.00^{+0.00}_{-0.00}$	201^{+3}_{-3}
1152+3400	$20.00^{+0.07}_{-0.07}$	5^{+1}_{-1}	$3.4^{+0.2}_{-0.1}$	$0.01^{+0.00}_{-0.00}$	333^{+6}_{-6}
0021+0052	$19.59^{+0.07}_{-0.07}$	130^{+4}_{-3}	$5.0^{+0.1}_{-0.1}$	$0.22^{+0.01}_{-0.01}$	100^{+2}_{-2}
1122+6154	$19.98^{+0.08}_{-1.85}$	7^{+1}_{-26}	$3.4^{+0.2}_{-0.2}$	$0.00^{+1.13}_{-0.00}$	259^{+4}_{-5}
0925+1403	$19.79^{+0.07}_{-0.08}$	8^{+1}_{-1}	$3.0^{+0.2}_{-0.2}$	$0.03^{+0.00}_{-0.00}$	229^{+5}_{-5}
0917+3152	$19.00^{+0.07}_{-0.07}$	60^{+3}_{-3}	$3.5^{+0.3}_{-0.2}$	$0.01^{+0.01}_{-0.01}$	275^{+8}_{-8}
1025+3622	$19.40^{+0.07}_{-0.07}$	110^{+3}_{-4}	$4.1^{+0.2}_{-0.3}$	$0.00^{+0.01}_{-0.00}$	228^{+7}_{-5}
1440+4619	$19.18^{+0.08}_{-0.08}$	259^{+4}_{-4}	$5.0^{+0.1}_{-0.1}$	$0.23^{+0.03}_{-0.03}$	117^{+2}_{-2}
1429+0643	$20.39^{+0.08}_{-0.08}$	15^{+2}_{-2}	$3.4^{+0.1}_{-0.1}$	$0.00^{+0.00}_{-0.00}$	392^{+3}_{-3}
1428+1653	$16.04^{+1.55}_{-0.09}$	168^{+5}_{-11}	$5.7^{+0.2}_{-0.4}$	$0.10^{+0.02}_{-0.09}$	205^{+20}_{-4}
2237+1336	$19.88^{+0.15}_{-0.13}$	258^{+44}_{-10}	$4.9^{+0.2}_{-1.1}$	$1.14^{+0.86}_{-0.33}$	140^{+12}_{-8}
1454+4528	$16.44^{+0.36}_{-0.09}$	-171^{+4}_{-4}	$5.4^{+0.1}_{-0.1}$	$4.78^{+0.17}_{-0.34}$	427^{+10}_{-8}
1018+4106	$19.60^{+0.07}_{-0.07}$	49^{+4}_{-4}	$3.8^{+0.2}_{-0.2}$	$0.07^{+0.04}_{-0.04}$	268^{+12}_{-11}
0751+1638	$19.39^{+0.07}_{-0.08}$	121^{+17}_{-20}	$4.4^{+0.3}_{-1.3}$	$0.17^{+0.34}_{-0.13}$	326^{+31}_{-29}
0822+2241	$20.54^{+0.11}_{-0.18}$	6^{+3}_{-2}	$3.0^{+0.1}_{-0.2}$	$0.01^{+0.02}_{-0.00}$	363^{+10}_{-19}
1339+1516	$19.00^{+0.07}_{-0.07}$	100^{+4}_{-4}	$3.1^{+0.6}_{-0.2}$	$4.86^{+0.11}_{-0.23}$	345^{+5}_{-5}
0938+5428	$20.60^{+0.08}_{-0.08}$	15^{+2}_{-2}	$4.6^{+0.2}_{-0.2}$	$0.08^{+0.01}_{-0.01}$	64^{+15}_{-10}
0055−0021	$20.40^{+0.07}_{-0.07}$	60^{+3}_{-4}	$4.2^{+0.1}_{-0.1}$	$0.07^{+0.02}_{-0.02}$	322^{+17}_{-17}

Note. Column descriptions: (2) H I column density of the outflowing H I shell; (3) outflowing velocity of the H I shell; (4) H I gas temperature including turbulent motion as well as the true temperature; (5) dust optical depth; and (6) 1σ width of the Gaussian profile of the intrinsic Lyα line. These 23 galaxies are sorted by decreasing $f_{\rm esc}^{\rm Ly\alpha}$ from top to bottom.

In the model, Lyα photons were generated by a source fully surrounded by a spherical dusty H I gas shell that scattered/absorbed the Lyα photons. The intrinsic Lyα line has a Gaussian profile with width σ. The shell is described by four parameters: (i) outflow velocity $v_{\rm exp}$, (ii) H I column density $N_{\rm H\,I}$, (iii) temperature T (including turbulent motion as well as the true temperature), and (iv) dust optical depth τ_d. Generally, these parameters affect the Lyα profile as follows: a larger outflow velocity and a smaller $N_{\rm H\,I}$ will decrease the red-peak velocity, a higher temperature will generally broaden the line profile, and a larger dust optical depth will decrease the line strength. Then, we find the best-fit model parameters (σ, $v_{\rm exp}$, $N_{\rm H\,I}$, T, τ_d) and calculate the errors of the parameters using the Markov Chain Monte Carlo (MCMC) method. We refer the reader to Gronke et al. (2015) and Paper I for details of the model and the fitting method.

In Paper I, we showed the fitting results for 12 Green Peas. The model fit nine profiles very well, but failed in the other three profiles. Here we show the fitting results for another 23 Green Peas (out of the 31 additional Green Peas) with sufficient S/N in their Lyα profiles. The model fit the observed profiles very well in many cases (Figure 9). The best-fit parameters are shown in Table 4. We discussed a few interesting fitting results below.

(1) H I column density. In Paper I, we found that $f_{\rm esc}^{\rm Ly\alpha}$ anti-correlates with the best-fit $N_{\rm H\,I}$ for the 12 Green Peas. Here we show the relation between $f_{\rm esc}^{\rm Ly\alpha}$ and the best-fit $N_{\rm H\,I}$ in Figure 10 for the combined sample of 35 Green Peas. The result confirms the anti-correlation between $f_{\rm esc}^{\rm Ly\alpha}$ and $N_{\rm H\,I}$. For the three cases (GP1424+4217, GP1133+6514, and GP1219+1526, marked by large blue circles) where the fitting procedure failed, we plot the $N_{\rm H\,I}$ obtained by manually adjusting the model parameters to match the observed depth of the "valley" and the relative heights of the blue and red peaks (see Section 6 of Paper I). For GP1454+4528 (marked by a red square) with gas inflow, the fitting was bad. For the two galaxies marked by large cyan triangles, the best-fit $N_{\rm H\,I}$ are not constrained. If the three galaxies marked by the square and triangle are excluded, the Spearman correlation coefficient for the relation of $f_{\rm esc}^{\rm Ly\alpha}$ and $N_{\rm H\,I}$ is $r = -0.59$ (P = 4e–4). If all six galaxies marked by the large circle, square, and triangle are excluded, the Spearman correlation coefficient is $r = -0.52$ (P = 4e–3). This result is consistent with studies of high-redshift LAEs that suggested LAEs have lower $N_{\rm H\,I}$ than non-LAEs (e.g., Erb et al. 2014; Shibuya et al. 2014; Hashimoto et al. 2015). Therefore, the low column density of H I gas is a key factor in Lyα escape.

(2) Intrinsic Lyα line width. The intrinsic Lyα line Gaussian width σ is about two to three times larger than the Hα Gaussian width in many cases, as we discussed in Paper I. In four cases, the best-fit σ is narrow and comparable to the Hα width because the best-fit profile only has a single peak. The wide intrinsic Lyα line profile can be due to important radiative transfer effects that broaden Lyα profile near to the source, before the processes attributed to the outflowing H I shell.

(3) Outflow velocities. The best-fit shell outflow velocities are mostly between 5 and 170 km s^{-1}, which are generally smaller than the outflow velocities measured from the low-ionized UV absorption lines (H. Yang et al. 2017, in preparation). This may suggest that the low-ionized absorption

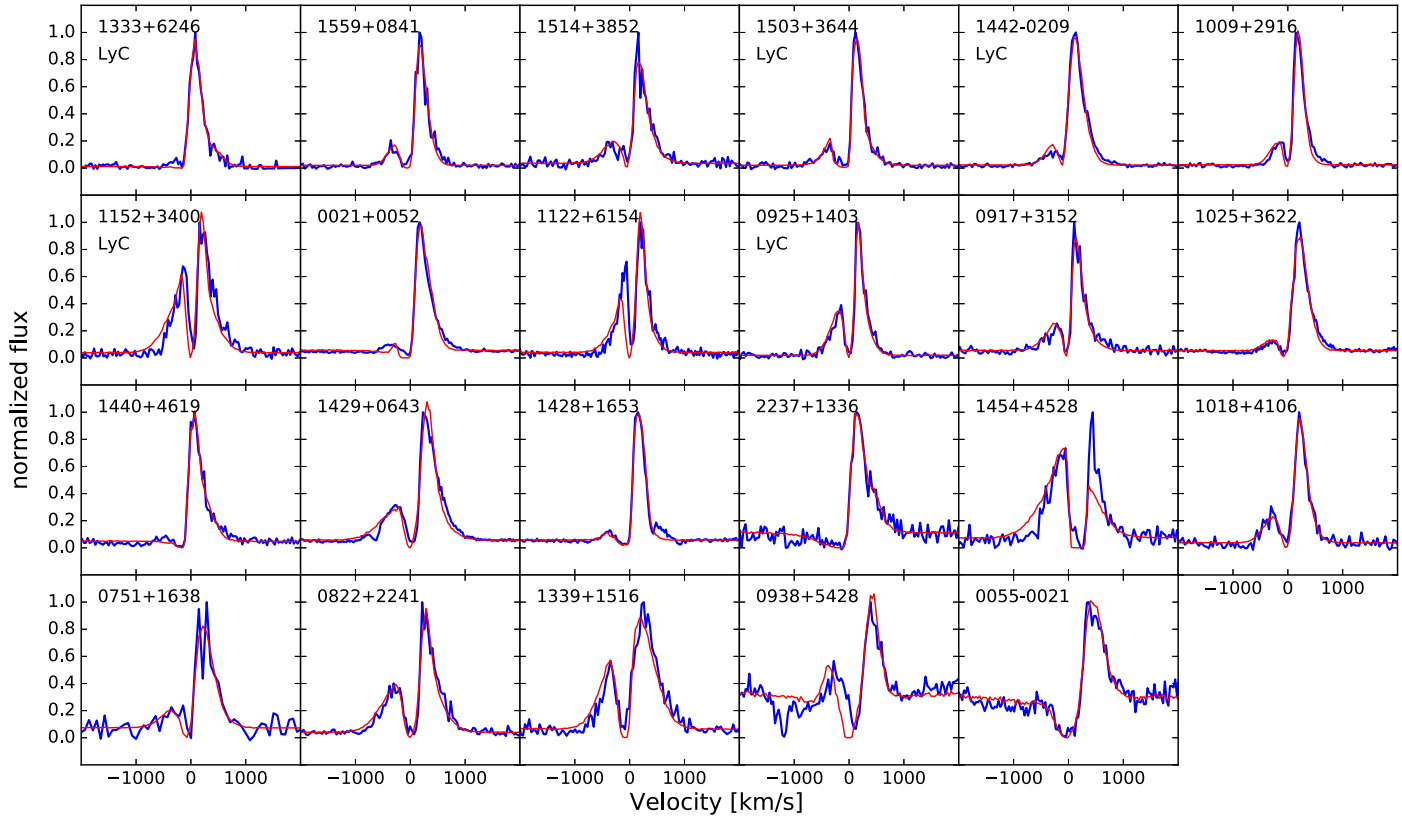

Figure 9. Observed Lyα profiles (blue lines) and best-fit Lyα profiles (red lines) for 23 Green Peas with good S/N in their Lyα profiles. In Paper I, we showed the radiative transfer model fitting results for another 12 Green Peas. These galaxies are sorted by decreasing $f_{\rm esc}^{\rm Ly\alpha}$ from left to right, and from top to bottom.

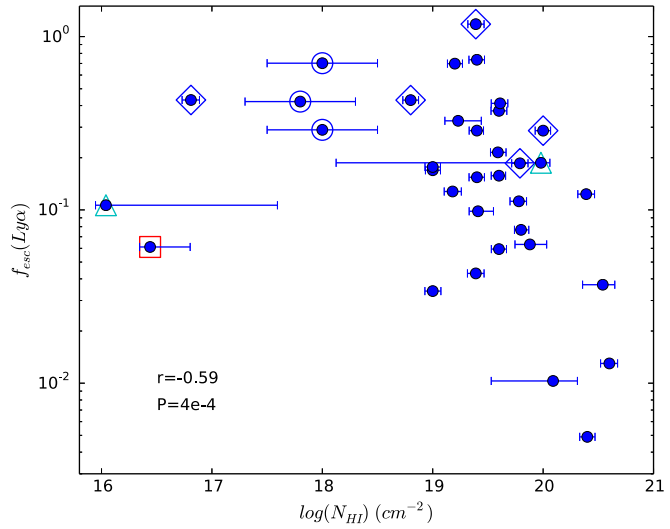

Figure 10. Relation between $f_{\rm esc}^{\rm Ly\alpha}$ and the best-fit $N_{\rm H\,I}$ from the radiative transfer model. Five known LyC leakers are marked by large diamonds. For the three cases (GP1424+4217, GP1133+6514, and GP1219+1526, marked by large blue circles) where the fitting procedure failed, we plot the $N_{\rm H\,I}$ obtained by manually adjusting the model parameters to match the observed depth of the "valley" and the relative heights of the blue and red peaks (see Section 6 of Paper I). For GP1454+4528 (marked by a large red square) with gas inflow, the fitting is bad (see Figure 8). For the two galaxies marked by large cyan triangles (GP1428+1653 and GP1122+6154), the best-fit $N_{\rm H\,I}$ are not constrained. The Spearman correlation coefficient is calculated without the three galaxies marked by square and triangle.

lines trace a different gas component from the H I gas. We also noticed that for six profiles with strong blue peaks, the best-fit shell outflow velocities are smaller than 20 km s^{-1}. In GP1454+4528, the outlier discussed in Section 4.1, the H I gas shell is inflowing with a best-fit velocity of 171 km s^{-1}.

(4) The three failed cases. In Paper I, the model failed in three profiles with positive velocities at the line "valley." We later improved the model by adding a shift of the velocity zero point as a free parameter of the fitting. The improved model can fit these three profiles very well, but the shifts of the velocity zero points are about 90–150 km s^{-1} which are too large to be due to the errors of wavelength calibration. Those large shifts may be explained by some additional radiative transfer effects before the Lyα photons meet the H I gas shell.

Although the shell model captures many real radiative transfer effects and can fit the Lyα profiles very well, we should be cautious about the interpretation of the best-fit parameters. A simple shell model can mimic more complex real physical properties (Gronke et al. 2016). For example, a low $N_{\rm H\,I}$ model can mimic a model in which the gas is clumpy and the covering factor is low (Gronke & Dijkstra 2016). In this case, the best-fit $N_{\rm H\,I}$ value is a simple approximation of the overall H I column densities. Interestingly, the best-fit $N_{\rm H\,I}$ of the five LyC leakers are about 10^{17-20} cm^{-2}, larger than the $N_{\rm H\,I}$ that permit LyC escape. It suggests that their LyC emission probably escape through some holes in the ISM with much lower $N_{\rm H\,I}$.

7. Predicting the Lyα Escape Fraction

As we said in the Introduction, one major reason for studying Lyα escape is to use Lyα lines to probe reionization. A fraction ($f_{\rm esc}^{\rm Ly\alpha}$) of intrinsic Ly$\alpha$ photons first escape out of an LAE, then they go through the IGM where they can be further scattered by H I, and the remaining photons can finally be

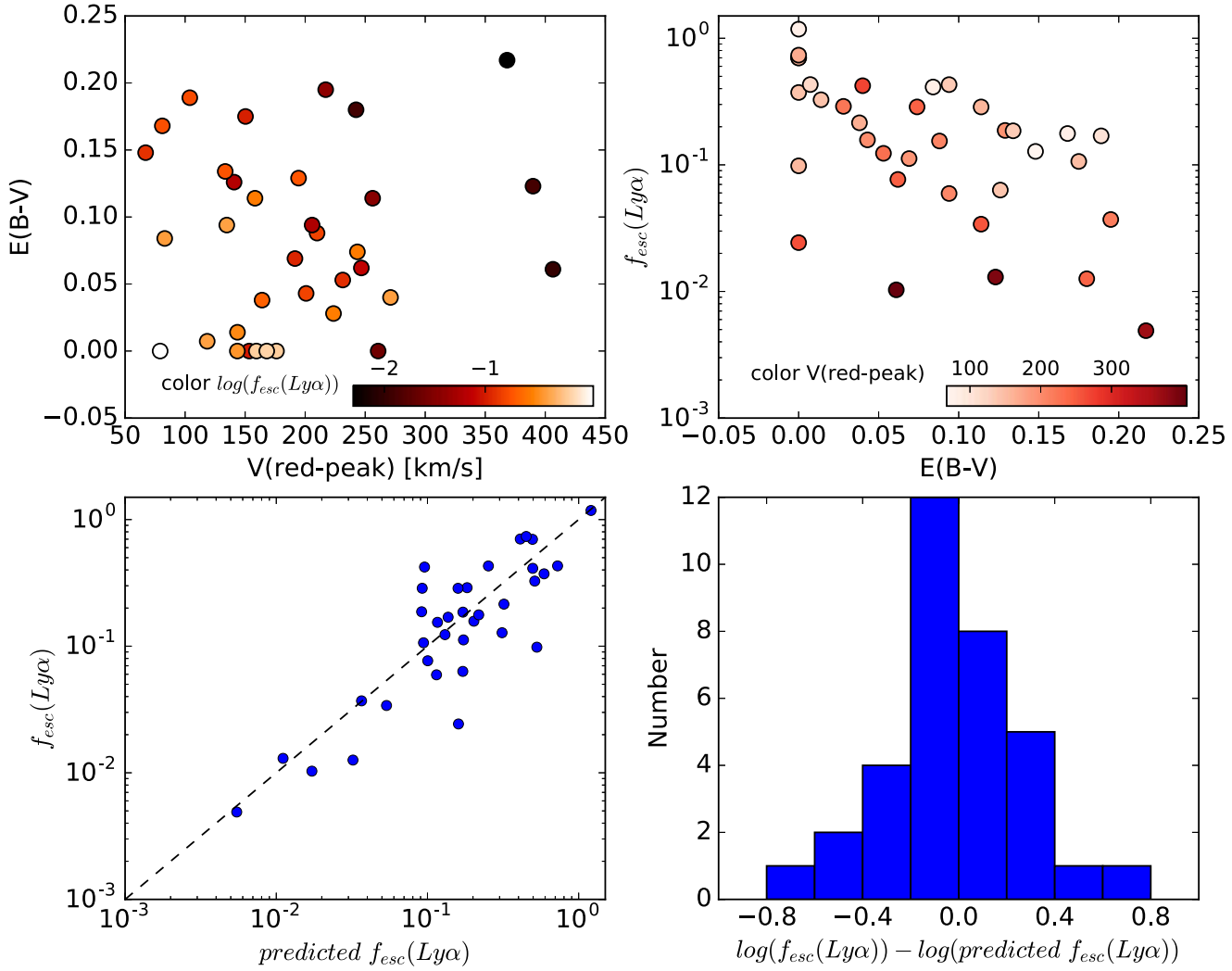

Figure 11. Top left: the relation of $E(B-V)$ vs. V(red-peak). The color bar shows the $\log(f_{\rm esc}^{\rm Ly\alpha})$ value. Top right: the relation of $f_{\rm esc}^{\rm Ly\alpha}$ and $E(B-V)$. The color bar shows the V(red-peak) value. Bottom left: the comparison of observed and predicted $f_{\rm esc}^{\rm Ly\alpha}$. Here, the predicted $\log(f_{\rm esc}^{\rm Ly\alpha}) = a \times (E(B-V)/0.1) + b \times (V\,({\rm redpeak})/100) + c$. Bottom right: the histogram of the differences, $\log(f_{\rm esc}^{\rm Ly\alpha})$ – log(predicted $f_{\rm esc}^{\rm Ly\alpha}$).

observed as a Lyα line. So, the IGM transmission can be measured from the observed Lyα line flux if we know the intrinsic Lyα line flux and $f_{\rm esc}^{\rm Ly\alpha}$, i.e., IGM Transmission = (Observed Lyα)/(Intrinsic Lyα $\times$ $f_{\rm esc}^{\rm Ly\alpha}$). In the near future, *JWST* will be able to measure the observed Lyα line and derive the intrinsic Lyα line from the observed Hα line for galaxies in the epoch of reionization. If the remaining factor, $f_{\rm esc}^{\rm Ly\alpha}$, can be predicted from other observed galactic properties, then each Lyα line can be used as an IGM probe on its line of sight. With this sample of Green Peas, we have found correlations between $f_{\rm esc}^{\rm Ly\alpha}$ and Lyα kinematic features, dust extinction, metallicity, stellar mass, and H I column density. So, can we select a few observable factors and fit an empirical relation to predict $f_{\rm esc}^{\rm Ly\alpha}$?

Physically, Lyα escape depends on the properties of dust and H I gas, so we should select the factors that can indicate the properties of dust and H I gas. Dust extinction is relatively easy to measure and could be a useful factor. The Lyα kinematic features strongly depend on the column density and kinematics of H I gas and could be another useful factor. Among several Lyα kinematic features, the Lyα red-peak velocity is easier and more robust to measure than the blue-peak velocity, which might be removed by absorption, and the line width, which depends on the spectra resolution. The other three factors—metallicity, stellar mass, and H I column density from the fitting of the Lyα profile—are difficult to measure and the uncertainties are large. Furthermore, both dust extinction and Lyα V(red-peak) show relatively tight anti-correlations with $f_{\rm esc}^{\rm Ly\alpha}$. So, we fit a linear empirical relation to predict $f_{\rm esc}^{\rm Ly\alpha}$ from the dust extinction and the V(red-peak) of the Lyα profile.

In Figure 11, we first show the relations of $f_{\rm esc}^{\rm Ly\alpha}$, $E(B-V)$, and V(red-peak). In the diagram of $E(B-V)$ versus V(red-peak), objects are color-coded by $f_{\rm esc}^{\rm Ly\alpha}$. We can see that (i) $E(B-V)$ and V(red-peak) do not show a correlation and (ii) the Green Peas with lower dust extinction and smaller V(red-peak) have larger $f_{\rm esc}^{\rm Ly\alpha}$. In the diagram of $f_{\rm esc}^{\rm Ly\alpha}$ versus $E(B-V)$, objects are color-coded by V(red-peak). Those Green Peas with large V(red-peak) generally have smaller $f_{\rm esc}^{\rm Ly\alpha}$ than the others *with the same E (B − V)*. Then, we fit 37 Green Peas with both V(red-peak) and $E(B-V)$ measurements. Two Green Peas, GP1454+4528 with gas inflow and GP0749+3337 with the largest V(red-peak), are outliers of the fitting, so we remove these two objects. The final

best-fit relation of 35 Green Peas is

$$\log(f_{\rm esc}^{\rm Ly\alpha}) = a \times (E(B-V)/0.1) + b \times (V({\rm redpeak})/100) + c,$$

where ($a = -0.437$, $b = -0.483$, $c = 0.464$). In the bottom two panels of Figure 11, we compare the observed and the predicted $f_{\rm esc}^{\rm Ly\alpha}$ and show the histogram of the differences, log ($f_{\rm esc}^{\rm Ly\alpha}$) – log(predicted $f_{\rm esc}^{\rm Ly\alpha}$). The standard deviation of this relation is 0.3 dex.

Now we have a relation to predict $f_{\rm esc}^{\rm Ly\alpha}$ from the dust extinction and Lyα V(red-peak). If *JWST* measures the observed Lyα flux, observed Hα flux, dust extinction, and Lyα V(red-peak) of a $z > 7$ LAE, then we can infer the IGM transmission along this line of sight using the formula IGM Transmission = (Observed [Lyα])/(Intrinsic $Ly\alpha \times f_{\rm esc}^{\rm Ly\alpha}$), where the "Intrinsic Lyα" is calculated from dust extinction-corrected Hα flux, and $f_{\rm esc}^{\rm Ly\alpha}$ is calculated from the empirical relation.

The IGM measured by this method is the "true" IGM far from the LAE, which is in contrast to the CGM. The "true" IGM only affects the strength of the Lyα red peak through the damped absorption factor of $e^{-\tau}$, where τ is the optical depth of the IGM H I gas along the line of sight, and its effect on the velocity of the narrow Lyα red peak is negligible. Some simulations suggested that the H I gas in the CGM can be very close to the Lyα photons in frequency, so the CGM H I gas can resonantly scatter and/or absorb Lyα photons at V(red-peak) $< 160\,{\rm km\,s^{-1}}$ (Laursen et al. 2011; Dijkstra 2014) and change the V(red-peak) of the Lyα profile. In fact those scatterings by the CGM are part of the Lyα escape process before Lyα photons reach the "true" IGM. So, the influence of CGM gas is already considered in the empirical relation.

This empirical relation has important implications for reionization tests with Lyα lines. Some observations suggested that the fraction of Lyα emission line in LBGs drops rapidly at $z > 6.5$ (e.g., Hayes et al. 2011; Pentericci et al. 2014; Tilvi et al. 2014). This could be due to small number statistics. But if this signal is real, it suggests that either (i) the "true" IGM optical depth increases rapidly or (ii) the optical depth of the ISM and CGM increases rapidly. Using our empirical relation, we can measure the optical depth of the "true" IGM and distinguish between these two possibilities.

Some recent observations suggest that five $z \sim 7$ galaxies show very small velocity offsets of about 20–150 $\rm km\,s^{-1}$ between Lyα and [C II] emission lines (Bradač et al. 2017; Pentericci et al. 2016). Those small V(red-peak) values may indicate that the Lyα escape fractions are high, and the optical depths of the ISM and CGM are small.

One caveat is with regard to whether the empirical relation derived from low-z analogs is applicable to high-z LAEs. The properties of the ISM and CGM likely evolve between the low-z LAEs (Green Peas) and the LAEs in the epoch of reionization. However, since the physics of Lyα resonant scattering is the same in both low and high z, increasing the H I gas column density in the ISM probably does not change how $N_{\rm H\,I}$ affects the Lyα profile. So, the empirical relation is very likely applicable to $z > 6$ LAEs.

8. Conclusion

We studied Lyα escape in a statistical sample of Green Peas with *HST*/COS Lyα spectra. About two-thirds of Green Peas show strong Lyα emission lines. Many Green Peas show double-peaked Lyα line profiles, but the Lyα profiles are diverse. These Green Peas have well-measured galactic properties from SDSS optical spectra, so we investigated the dependence of Lyα escape on dust extinction, metallicity, stellar mass, galaxy morphology, and [O III]/[O II] ratio. We also fit their Lyα profiles with the H I shell radiative transfer model. Finally, we derived an empirical relation to predict the Lyα escape fraction. Our major conclusions are as follows:

1. With a statistical sample of 43 Green Peas that cover the whole ranges of dust extinction and metallicity properties of Green Peas, we found that about two-thirds of Green Peas are strong Lyα line emitters with EW(Lyα) distribution consistent with high-z LAEs. This confirmed that Green Peas generally are the best analogs of high-z LAEs in the nearby universe.
2. $f_{\rm esc}^{\rm Ly\alpha}$ shows anti-correlations with several Lyα kinematic features—the blue peak velocity, the red peak velocity, the peak separation, and the FWHM(red) of the Lyα profile. These Lyα kinematic features are sensitive to the column density and the kinematics of H I gas. As more scatterings in H I gas can make the Lyα velocity offsets larger and the Lyα profile broader, these correlations strongly suggest that low $N_{\rm H\,I}$ and fewer scatterings help Lyα photons escape.
3. With a large sample, we found many *correlations* regarding the dependence of Lyα escape on galactic properties—$f_{\rm esc}^{\rm Ly\alpha}$ generally increases at lower dust extinction, lower metallicity, lower stellar mass, and higher [O III]/[O II] ratio. $f_{\rm esc}^{\rm Ly\alpha}$ does not have an obvious relation with the UV morphology of Green Peas.
4. The single-shell radiative transfer model can reproduce most Lyα profiles of Green Peas. The best-fit $N_{\rm H\,I}$ anti-correlates with $f_{\rm esc}^{\rm Ly\alpha}$, indicating that low $N_{\rm H\,I}$ is key to Lyα escape.
5. We fit an empirical linear relation between $f_{\rm esc}^{\rm Ly\alpha}$, dust extinction, and the Lyα red peak velocity. This relation can be used to predict the $f_{\rm esc}^{\rm Ly\alpha}$ of LAEs and isolate the effect of IGM scatterings from Lyα escape. As *JWST* can measure the dust extinction and Lyα red peak velocity of some $z > 7$ LAEs, this relation makes it possible to measure the H I column density of the IGM along the line of sight of each LAE and to probe the reionization with their Lyα lines.

We thank David Sobral, Edmund Christian Herenz, Kimihiko Nakajima, Alaina Henry, and the referee for very helpful comments. The imaging and spectroscopy data are based on observations with the NASA/ESA *Hubble Space Telescope*, obtained at the Space Telescope Science Institute, which is operated by the Association of Universities for Research in Astronomy (AURA), Inc., under NASA contract NAS 5-26555. Some of the data presented in this paper were obtained from the Mikulski Archive for Space Telescopes (MAST). STScI is operated by the Association of Universities for Research in Astronomy, Inc., under NASA contract NAS 5-26555. Support for MAST for non-*HST* data is provided by the NASA Office of Space Science via grant NNX09AF08G and by other grants and contracts. H.Y. acknowledges support from the China Scholarship Council. H.Y. and J.X.W. thank support from NSFC 11233002 and 11421303, and the CAS Frontier Science Key Research Program (QYZDJ-SSW-SLH006).

This work has also been supported in part by NSF grant AST-1518057 and by support for *HST* program #14201.

ORCID iDs

Huan Yang https://orcid.org/0000-0003-2260-7420
Sangeeta Malhotra https://orcid.org/0000-0002-9226-5350
Max Gronke https://orcid.org/0000-0003-2491-060X
Claus Leitherer https://orcid.org/0000-0003-2685-4488
V. Tilvi https://orcid.org/0000-0001-8514-7105
Junxian Wang https://orcid.org/0000-0002-4419-6434

References

Ahn, S.-H., Lee, H.-W., & Lee, H. M. 2001, ApJ, 554, 604
Alexandroff, R. M., Heckman, T. M., Borthakur, S., Overzier, R., & Leitherer, C. 2015, ApJ, 810, 104
Amorín, R. O., Pérez-Montero, E., & Vílchez, J. M. 2010, ApJL, 715, L128
Atek, H., Kunth, D., Schaerer, D., et al. 2014, A&A, 561, A89
Atek, H., Schaerer, D., & Kunth, D. 2009, A&A, 502, 791
Bond, N. A., Feldmeier, J. J., Matković, A., et al. 2010, ApJL, 716, L200
Borthakur, S., Heckman, T. M., Leitherer, C., & Overzier, R. A. 2014, Sci, 346, 216
Bradač, M., Garcia-Appadoo, D., Huang, K.-H., et al. 2017, ApJL, 836, L2
Calzetti, D., Armus, L., Bohlin, R. C., et al. 2000, ApJ, 533, 682
Cardamone, C., Schawinski, K., Sarzi, M., et al. 2009, MNRAS, 399, 1191
Charlot, S., & Fall, S. M. 1993, ApJ, 415, 580
Chonis, T. S., Blanc, G. A., Hill, G. J., et al. 2013, ApJ, 775, 99
Cowie, L. L., Barger, A. J., & Hu, E. M. 2011, ApJ, 238, 136
de Barros, S., Vanzella, E., Amorín, R., et al. 2016, A&A, 585, A51
Deharveng, J.-M., Small, T., Barlow, T. A., et al. 2008, ApJ, 680, 1072
Dey, A., Spinrad, H., Stern, D., Graham, J. R., & Chaffee, F. H. 1998, ApJL, 498, L93
Dijkstra, M. 2014, PASA, 31, e040
Dijkstra, M., Gronke, M., & Venkatesan, A. 2016, ApJ, 828, 71
Dijkstra, M., Haiman, Z., & Spaans, M. 2006, ApJ, 649, 14
Erb, D. K., Steidel, C. C., Trainor, R., et al. 2014, ApJ, 795, 33
Finkelstein, S. L., Cohen, S. H., Malhotra, S., et al. 2009, ApJL, 703, L162
Finkelstein, S. L., Cohen, S. H., Moustakas, J., et al. 2011, ApJ, 733, 117
Finkelstein, S. L., Rhoads, J. E., Malhotra, S., Grogin, N., & Wang, J. 2008, ApJ, 678, 655
Fitzpatrick, E. L. 1999, PASP, 111, 63
Gawiser, E., Francke, H., Lai, K., et al. 2007, ApJ, 671, 278
Gawiser, E., van Dokkum, P. G., Gronwall, C., et al. 2006, ApJL, 642, L13
Giavalisco, M., Koratkar, A., & Calzetti, D. 1996, ApJ, 466, 831
Gordon, K. D., Clayton, G. C., Misselt, K. A., Landolt, A. U., & Wolff, M. J. 2003, ApJ, 594, 279
Gronke, M., Bull, P., & Dijkstra, M. 2015, ApJ, 812, 123
Gronke, M., & Dijkstra, M. 2016, ApJ, 826, 14
Gronke, M., Dijkstra, M., McCourt, M., & Oh, S. P. 2016, ApJL, 833, L26
Hansen, M., & Oh, S. P. 2006, MNRAS, 367, 979
Hashimoto, T., Ouchi, M., Shimasaku, K., et al. 2013, ApJ, 765, 70
Hashimoto, T., Verhamme, A., Ouchi, M., et al. 2015, ApJ, 812, 157
Hayes, M., Östlin, G., Duval, F., et al. 2014, ApJ, 782, 6
Hayes, M., Östlin, G., Mas-Hesse, J. M., et al. 2005, A&A, 438, 71
Hayes, M., Östlin, G., Schaerer, D., et al. 2013, ApJL, 765, L27
Hayes, M., Schaerer, D., Östlin, G., et al. 2011, ApJ, 730, 8
Heckman, T. M., Borthakur, S., Overzier, R., et al. 2011, ApJ, 730, 5
Henry, A., Scarlata, C., Martin, C. L., & Erb, D. 2015, ApJ, 809, 19
Hu, E. M., Cowie, L. L., & McMahon, R. G. 1998, ApJL, 502, L99
Izotov, Y. I., Guseva, N. G., & Thuan, T. 2011, ApJ, 728, 161
Izotov, Y. I., Schaerer, D., Thuan, T. X., et al. 2016, MNRAS, 461, 3683
Izotov, Y. I., Stasińska, G., Meynet, G., Guseva, N. G., & Thuan, T. X. 2006, A&A, 448, 955
James, B. L., Aloisi, A., Heckman, T., Sohn, S. T., & Wolfe, M. A. 2014, ApJ, 795, 109
Jaskot, A. E., & Oey, M. S. 2014, ApJ, 791, 19L
Kashikawa, N., Shimasaku, K., Matsuda, Y., et al. 2011, ApJ, 734, 119
Kennicutt, R. C., & Evans, N. J. 2012, ARA&A, 50, 531
Kunth, D., Mas-Hess, J. M., Terlevich, E., et al. 1998, A&A, 334, 11
Laursen, P., Duval, F., & Östlin, G. 2013, ApJ, 766, 124
Laursen, P., Sommer-Larsen, J., & Razoumov, A. O. 2011, ApJ, 728, 52
Leitet, E., Bergvall, N., Hayes, M., Linné, S., & Zackrisson, E. 2013, A&A, 553, A106
Leitherer, C., Hernandez, S., Lee, J. C., & Oey, M. S. 2016, ApJ, 823, 64
Leitherer, C., Tremonti, C. A., Heckman, T. M., & Calzetti, D. 2011, AJ, 141, 37
Levesque, E. M., & Leitherer, C. 2013, ApJ, 779, 170
Lupton, R., Blanton, M. R., Fekete, G., et al. 2004, PASP, 116, 133
Ly, C., Malkan, M. A., Nagao, T., et al. 2014, ApJ, 780, 122
Malhotra, S., & Rhoads, J. E. 2004, ApJL, 617, L5
Malhotra, S., Rhoads, J. E., Finkelstein, S. L., et al. 2012, ApJL, 750, L36
Mas-Hesse, J. M., Kunth, D., Tenorio-Tagle, G., et al. 2003, ApJ, 598, 858
Matthee, J., Sobral, D., Santos, S., et al. 2015, MNRAS, 451, 400
Matthee, J. J. A., Sobral, D., Swinbank, A. M., et al. 2014, MNRAS, 440, 2375
McLinden, E. M., Finkelstein, S. L., Rhoads, J. E., et al. 2011, ApJ, 730, 136
McLinden, E. M., Rhoads, J. E., Malhotra, S., et al. 2014, MNRAS, 439, 446
Momose, R., Ouchi, M., Nakajima, K., et al. 2014, MNRAS, 442, 110
Neufeld, D. A. 1990, ApJ, 350, 216
Östlin, G., Hayes, M., Duval, F., et al. 2014, ApJ, 797, 11
Östlin, G., Hayes, M., Kunth, D., et al. 2009, AJ, 138, 923
Ouchi, M., Shimasaku, K., Furusawa, H., et al. 2003, ApJ, 582, 60
Peña-Guerrero, M. A., & Leitherer, C. 2013, AJ, 146, 158
Peng, C. Y., Ho, L. C., Impey, C. D., & Rix, H.-W. 2010, AJ, 139, 2097
Pentericci, L., Carniani, S., Castellano, M., et al. 2016, ApJL, 829, L11
Pentericci, L., Vanzella, E., Fontana, A., et al. 2014, ApJ, 793, 113
Pirzkal, N., Malhotra, S., Rhoads, J. E., & Xu, C. 2007, ApJ, 667, 49
Rhoads, J. E., Dey, A., Malhotra, S., et al. 2003, AJ, 125, 1006
Rhoads, J. E., Malhotra, S., Dey, A., et al. 2000, ApJL, 545, L85
Rivera-Thorsen, T. E., Hayes, M., Östlin, G., et al. 2015, ApJ, 805, 14
Santos, S., Sobral, D., & Matthee, J. 2016, MNRAS, 463, 1678
Scarlata, C., Colbert, J., Teplitz, H. I., et al. 2009, ApJ, 705, 98L
Schaerer, D., Hayes, M., Verhamme, A., & Teyssier, R. 2011, A&A, 531, A12
Schlafly, E. F., & Finkbeiner, D. F. 2011, ApJ, 737, 103
Shapley, A. E., Steidel, C. C., Pettini, M., & Adelberger, K. L. 2003, ApJ, 588, 65
Shapley, A. E., Steidel, C. C., Strom, A. L., et al. 2016, ApJL, 826, L24
Shibuya, T., Ouchi, M., Nakajima, K., et al. 2014, ApJ, 788, 74
Song, M., Finkelstein, S. L., Gebhardt, K., et al. 2014, ApJ, 791, 3
Stark, D. P., Ellis, R. S., & Ouchi, M. 2011, ApJL, 728, L2
Tilvi, V., Papovich, C., Finkelstein, S. L., et al. 2014, ApJ, 794, 5
Treu, T., Trenti, M., Stiavelli, M., Auger, M. W., & Bradley, L. D. 2012, ApJ, 747, 27
Verhamme, A., Orlitova, I., Schaerer, D., et al. 2017, A&A, 597, A13
Verhamme, A., Orlitová, I., Schaerer, D., & Hayes, M. 2015, A&A, 578, A7
Verhamme, A., Schaerer, D., & Maselli, A. 2006, A&A, 460, 397
Wang, J.-X., Malhotra, S., Rhoads, J. E., Zhang, H.-T., & Finkelstein, S. L. 2009, ApJ, 706, 762
Wofford, A., Leitherer, C., & Salzer, J. 2013, ApJ, 765, 118
Xia, L., Malhotra, S., Rhoads, J., et al. 2012, AJ, 144, 28
Yang, H., Malhotra, S., Gronke, M., et al. 2016, ApJ, 820, 130
Yang, H., Malhotra, S., Rhoads, J. E., et al. 2017, ApJ, 838, 4
Zheng, Z.-Y., Malhotra, S., Rhoads, J. E., et al. 2016, ApJS, 226, 23